THESIS FOR THE DEGREE OF DOCTOR OF PHILOSOPHY

Removal of contaminants by jumping droplets from superhydrophobic surfaces – a numerical study

Konstantinos Konstantinidis

Department of Mechanics and Maritime Sciences
Chalmers University of Technology
Gothenburg, Sweden, 2025

Removal of contaminants by jumping droplets from superhydrophobic surfaces – a numerical study

Konstantinos Konstantinidis

ISBN: 978-91-8103-149-2
Technical Report No. 5607
ISSN 0346-718X
Department of Mechanics and Maritime Sciences

Chalmers University of Technology
SE-412 96 Gothenburg, Sweden
Phone: +46 (0)31 772 1000
www.chalmers.se

Printed by Chalmers Reproservice
Gothenburg, Sweden, January 2025

To my family, friends and colleagues

Abstract

Superhydrophobic surfaces are advantageous in numerous applications due to their anti-icing, water-repellent and enhanced heat-transfer abilities. A great number of studies have been performed in order to improve those properties, with their self-cleaning ability standing out as their most desirable feature. This thesis focuses on passive self-cleaning mechanisms and uses advanced numerical simulations to characterize the properties of superhydrophobic surfaces and a series of fundamental phenomena that facilitate liquids and contaminant removal.

A detailed numerical framework has been developed in discrete steps, tackling the increased complexity that each separate study introduced. Initially, a volume of fluid (VOF) model is used to simulate droplets jumping from superhydrophobic surfaces, a phenomenon initiated when two or more droplets coalesce on a superhydrophobic surface. This part of the work was within the capillary-inertial dominated spectrum, where the droplets pertain the strongest capillarity. Simulations of coalescence and jumping of droplets of various sizes were performed, providing insights into the interaction of hydrodynamic forces and surface tension. The next step was the understanding and implementation of effective contact angle hysteresis and explore its influence on the jumping efficiency. Hysteresis, introduced either by static or dynamic modeling of the contact angle, increased the energy dissipation of a surface and showcased re-attachment events for the merged droplet.

During the course of the project, another study reported the removal of a particle by a single droplet. This self-cleaning mechanism occurs when a droplet initiates spreading on a hydrophilic particle, capturing it in the process. Due to its oscillations, the droplet interacts with the superhydrophobic surface and the particle-droplet system jumps from the surface. To describe this phenomenon, a numerical study was performed using a combined VOF-immersed boundary method, with a special focus on formulating and implementing the capillary force attracting the particle. The latter formulation was validated benefiting from an experimental study, and a parameter study followed with regards to the properties of the involved phases and the wettability of the solids.

In the final part, pillar-shaped structures were introduced on the superhydrophobic surface to explore the effect of having structured surfaces on the particle-droplet coalescence and jumping. A comparison was performed be-

tween jumping from a smooth superhydrophobic surface and those from a pillared surface, showcasing the ability of the latter to achieve jumping and to undergo all the stages of the process. Finally, different configurations of pillars were tested, revealing that narrower and taller pillars with a sufficient spacing promote self-cleaning with the least dissipated energy.

Keywords: Superhydrophobic, self-cleaning, droplet jumping, interfacial phenomena, DNS, VOF, immersed boudnary method, CFD, particle removal

List of Publications

This thesis is based on the following publications:

[A] Konstantinos Konstantinidis, Johan Göhl, Andreas Mark, Srdjan Sasic, "**Coalescence-induced jumping of microdroplets on superhydrophobic surfaces – A numerical study.**". Can. J. Chem. Eng. 100, 3517–3530 (2022).

[B] Konstantinos Konstantinidis, Johan Göhl, Andreas Mark, Srdjan Sasic, "**Coalescence-induced jumping of droplets from superhydrophobic surfaces – The effect of contact-angle hysteresis.**". Phys. Fluids 34, 113302 (2022).

[C] Konstantinos Konstantinidis, Johan Göhl, Andreas Mark, Xiao Yan, Nenad Miljkovic, Srdjan Sasic, "**Particle–droplet coalescence and jumping on superhydrophobic surfaces – A direct numerical simulations study**". Phys. Fluids 36, 082117 (2024).

[D] Konstantinos Konstantinidis, Johan Göhl, Andreas Mark, Xiao Yan, Nenad Miljkovic, Srdjan Sasic, "**The role of surface microstructures in particle-droplet coalescence and jumping from superhydrophobic surfaces.**". Submitted to a scientific journal.

Acknowledgments

I would like to thank my main supervisor, professor Srdjan Sasic for his guidance and support throughout the period of the doctoral project. My co-supervisor associate professor Andreas Mark (Fraunhofer-Chalmers Centre), and Johan Göhl (Fraunhofer-Chalmers Centre), have also been instrumental in contributing their expertise and insights, together with crucial software support, for which I am deeply grateful. I would also like to express my thanks to professors Nenad Miljkovic from Illinois University and Xiao Yan from Chongqing University for noticing our work and deciding to contribute to the latter stages with their significant experience and expertise.

Furthermore, I am equally thankful to my colleagues and friends in the Fluid Dynamics division and the multiphase flow group, to whom I have already shared my gratitude, for their encouragement and motivation during these past years — and for just being there listening. Lastly, I am most grateful to my family for their unconditional love and support, which has been my constant source of strength.

Acronyms

AMR	–	Adaptive Mesh Refinement
CCF	–	Continuum Capillary Force
CFL	–	Courant–Friedrichs–Lewy or Courant number
CICSAM	–	Compressive Interface Capturing Scheme for Arbitrary Meshes
CSF	–	Continuum Surface Force
DNS	–	Direct Numerical Simulation
IBM	–	Immersed Boundary Method
MCL	–	Moving Contact Line
SIMPLEC	–	Semi-Implicit Method for Pressure Linked Equations-Consistent
VOF	–	Volume of Fluid

Nomenclature

$\hat{\mathbf{d}}$	unit vector for centerline of droplet/particle spheres	(-)
$\hat{\mathbf{n}}$	unit interface normal vector	(-)
$\mathbf{f}_{\mathrm{CCF}}$	capilary continuum body force	$(\mathrm{kg{\cdot}m^{-2}{\cdot}s^{-2}})$
$\mathbf{F}_{cap}$	capilary force	$(\mathrm{kg{\cdot}m{\cdot}s^{-2}})$
$\mathbf{F}_{CCF}$	total capilary continuum force	$(\mathrm{kg{\cdot}m{\cdot}s^{-2}})$
$\mathbf{F}_{IB}$	total hydrodynamic forces on solid from IBM	$(\mathrm{kg{\cdot}m{\cdot}s^{-2}})$
$\mathbf{f}_{SF}$	surface tension body force	$(\mathrm{kg{\cdot}m^{-2}{\cdot}s^{-2}})$
$\mathbf{I}$	particle moment of inertia	$(\mathrm{kg{\cdot}m^{2}})$
$\mathbf{n}$	interface normal vector	$(\mathrm{m^{-1}})$
$\mathbf{n}_{\mathrm{DS}}$	normal vector to solid surface	(-)
$\mathbf{n}_w$	normal wall direction	(m)
$\mathbf{r}_{V_i}$	distance of surface point from center of rotation	(m)
$\mathbf{t}_{\mathrm{dS}}$	hydrodynamic stresses on particle surface	$(\mathrm{kg{\cdot}m^{-1}{\cdot}s^{-2}})$
$\mathbf{t}_C$	tangential vector to solid surface towards direction of contact line velocity	(-)
$\mathbf{T}_{CCF}$	total torque from capillary continuum force	$(\mathrm{kg{\cdot}m^{2}{\cdot}s^{-2}})$
$\mathbf{t}_{Cl}$	tangential vector along the wall towards from the projection of the interface normal	(-)
$\mathbf{T}_{IB}$	total torque from hydrodynamic forces on solid from IBM	$(\mathrm{kg{\cdot}m^{2}{\cdot}s^{-2}})$

$\mathbf{t}_{int}$	tangential vector to the interface, away from the solid	(-)
$\mathbf{v}$	velocity	($\mathrm{m{\cdot}s^{-1}}$)
$\mathbf{v}_P$	particle velocity	($\mathrm{m{\cdot}s^{-1}}$)
K^*_{rot}	normalised oscillation kinetic energy of droplet	(-)
K^*_{rot}	normalised rotational kinetic energy of system	(-)
K^*_{tot}	normalised total kinetic energy normalised	(-)
K^*_{tra}	normalised translational kinetic energy of objects	(-)
K_i or $\mathrm{K}^*_{i,\,tra}$	normalised kinetic energy in direction i	(-)
K_{total} or K^*_{tot}	normalised total kinetic energy normalised	(-)
S_{lg}	normalised surface energy in the liquid–gas interface	(-)
ω_P	particle angular velocity	($\mathrm{rad{\cdot}s^{-1}}$)
$\overline{v}^*$	averaged normalized vertical velocity of droplet	(-)
$\overline{v}^*_{jump}$	normalized jumping velocity of droplet	(-)
A_{cont}	Contact area to solid surface	($\mathrm{m^2}$)
c_R	Number of cells per radius	(-)
f_{Hoff}	Hoffman function for Kistler dynamic contact angle model	(-)
$F_{pinning}$	Pinning or adhesion force	(N)
g	gravitational acceleration	($\mathrm{m{\cdot}s^{-2}}$)
h	height of pillars	(m)
l^*_{con}	arch length of spreading at ideal wetting position	(m)
l_{con}	arch length of spreading	(m)
p	pressure	($\mathrm{kg{\cdot}m^{-1}{\cdot}s^{-2}}$)
R or R_i or R_d	radius of initial droplets	(m)

R_c or R_{end}	radius of merged droplet	(m)
R_p	radius of particle	(m)
t	time	(s)
t_{CI}	capillary-inertial time scale	(s)
U_{CI}	normalized capillary-inertial velocity	(-)
v_{slip}	slip velocity at boudnary	($\mathrm{m{\cdot}s^{-1}}$)
w	width of pillars	(m)
a	angle of spreading	(°)

Greek Letters

β	spreading factor in epxonential rate of spreading with time (log-scale)	(-)
Φ	solid area fraction of wetted area over total surface area	(-)
α	volume fraction	(-)
χ	fraction of solid volume in cells	(-)
$\Delta\tau$	normalized time step	(-)
$\Delta\theta$	contact angle hysteresis	(°)
ΔE^*_{rel}	normalised available surface energy for particle-droplet jumping	(-)
ΔS	normalised available surface energy for coalescence of droplets	(-)
Δt	time step	(s)
Δx	cell size	(m)
κ	interface curvature	($\mathrm{m^{-1}}$)
λ	slip length	(m)
τ	normalized time	(-)

τ_{CI}	normalized capillary-inertial time	(-)
μ	dynamic viscosity	$(\mathrm{kg{\cdot}m^{-1}{\cdot}s^{-1}})$
ψ	angle of interface and capillary force diraction	$(^\circ)$
ρ	density	$(\mathrm{kg{\cdot}m^{-3}})$
σ	surface tension	$(\mathrm{kg{\cdot}s^{-2}})$
θ_{adv}	advancing contact angle	$(^\circ)$
θ_{dyn}	dynamic contact angle	$(^\circ)$
θ_{rec}	receding contact angle	$(^\circ)$

Dimensionless numbers

Ca	capillary number	(-)
Oh	Ohnesorge number	(-)
Re	Reynolds number	(-)
We	Weber number	(-)

Contents

Part I

Overview

CHAPTER 1

Introduction

This thesis addresses the modeling of self-cleaning processes at the micro-scale, that occur in the presence of droplets (wetting a superhydrophobic surface) and contaminant particles. It discusses the current industrial needs regarding surfaces exhibiting extraordinary phenomena, such as self-cleaning, expanding on the types of superhydrophobic surfaces available. The work argues that in order **to design superhydrophobic surfaces for self-cleaning, detailed numerical analysis is to be utilized.** Through simulations that reproduce the different mechanisms of self-cleaning, the work manages to **identify the different physical phenomena that occur at early stages of the mechanisms** and, therefore, it is able to fundamentally study all the stages of these mechanisms. The subsequent studies will **develop a continuum framework to understand the behavior of droplets when wetting a substrate and interacting with a contaminant**. Finally, the thesis will conclude with an investigation of specific properties, such as energy dissipation at different scales, contact-angle hysteresis on superhydrophobic surfaces, interactions with specific particle types and sizes, and interactions with surface structures that can hinder certain stages of self-cleaning.

1.1 Need for Innovative Surfaces

The project was conceived in response to current demands in industrial applications regarding surfaces often exposed to liquid films and droplets. To improve these interactions first there is a need to identify the problems. Surfaces that are exposed to outer environments can be subjected to rain droplets and water film floodings. With the swift removal of liquid from surfaces, processes can benefit from factors such as the improved air flow, the heat transfer efficiency, and the prevention of corrosion or salt depositions. Moreover droplets in motion can coalesce and agglomerate, removing other droplets, dirt particles or colloids. On the other hand, in condensation environments, like the condensation in a condenser heat-exchanger, droplets are beneficial since drop-wise condensation is more efficient than film condensation. However, the process requires the removal of droplets in an efficient way to offer space for new nucleations of condensing droplets. Research studies focused to the application of superhydrophobic surfaces, that exhibit high contact angles of 150° and higher, and reduced contact area with the droplets, as the most efficient solution of the identified issues[1].

By exhibiting high water repellency, superhydrophobic surfaces can provide highly desirable self-removal of droplets and other contaminants, and, therefore, they are promising for various industries. For instance, in the construction industry, superhydrophobic coatings can be applied on windows, building facades and rooftop panels[2], [3], significantly reducing maintenance costs by preventing dirt accumulation. In the automotive industry, these surfaces can be used on windshields, and improve the efficiency of condensers in heat exchangers, where the surface is in constant contact with water. Superhydrophobic surfaces facilitate heat transfer rates by drop-wise condensation[4], [5] and remove particles via self-cleaning behavior[6]–[10]. Additionally, superhydrophobic surfaces are crucial in the development of anti-icing coatings[11]–[13] for aircraft or in wind turbines, where ice accumulation is a significant issue, often addressed with other costly solutions. Finally, even the field for design of electronics[9] has considered superhydrophobic surfaces in order to enhance the performance of devices by self-cleaning properties that can reduce bacterial adhesion.

The wetting of a surface is broken down to a list of different interactions of a liquid with a solid, with the existence of a surrounding gas. These interactions span between different scales, starting from the molecular scale which

is a few nanometers, to the continuum scale which it is established at around 100 nanometers. Capillary forces dictate the balance of forces in wetting phenomena, while surface tension is responsible for the strength of the existing forces. The contact line, the triple-phase conjunction line of the different phases (the surrounding gas, the wetting liquid and the solid surface) is the location where the capillary forces act[14]. In the case of a droplet, they also account for the Laplace pressure of the droplet[15], which also affects the curvature of the droplet, and create balance in a static wetting configuration. In this system, an energy balance that minimizes the Gibbs free energy can compute the wetting area[16] and the liquid-gas interface area. For this calculation, one needs to provide the surface energy or surface tension of each pair of contacts (liquid–gas, solid–liquid, solid–gas) which is not straightforward to know at any occasion, while it can be highly dependent on the chemical variations of the solid surface. Therefore different means to simulate the capillary interactions are required.

1.2 Numerical simulations and surface wetting

Numerical simulations are essential for studying and designing superhydrophobic surfaces, particularly since experimental approaches can face various challenges. These difficulties arise due to the complex nature of the processes involved in wetting interactions, which combine the principles of fluid dynamics, surface properties, chemical composition and multi-scale features. Since the mechanisms behind self-cleaning processes of these surfaces are yet unclear, and depend on different physical principles, the explanation and quantification of these interactions pose challenges for experimental studies. Hence, it becomes difficult to isolate the individual phenomena such as dynamic behavior of contact angles, pinning and contact angle hysteresis[14], or droplet coalescence and spreading dynamics[16]. Experimental methods tend to focus on macroscopic outcomes, such as the overall removal of contaminants[17], without being able to directly observe in detail the interfacial and contact phenomena. On the other hand, numerical simulations offer a framework to control each contributing factor in self-cleaning, analyze them independently or in combinations, therefore providing insights into the fundamental mechanics taking place.

Moreover, the design process of surfaces will be aided by predicting how

they will perform under various conditions and droplet-substrate configurations. Simulations allow us to explore the performance limits and optimize surface characteristics, such as roughness, geometry, and wettability providing as a result possible improvements for the testing and manufacturing of surfaces. The focus is concentrated on the usage of models for the contact angle behavior. Superhydrophobic surfaces often possess geometrical features appearing on a surface. The features, which are responsible for roughness and other disparities of the surface, can instigate pinning and other contact line deformities[18]–[20], when their size is comparable to the length scales of the system. Therefore it is understood that there is a need to develop models which can capture i) the influence of micro-scale phenomena at the very vicinity of the contact line (intrinsic wettability) and ii) the influence of geometrical features appearing on a surface. The models suggested also need to be compared with numerical results that fully resolve the geometries of these so-called micro-structures, as well as with experimental results.

Numerical computations can also resolve with high fidelity multi-scale interactions of different fluid phases, enabling researchers to examine early-stage dynamics, such as droplet coalescence and capillary bridge formations[21]. Such studies highlight the essential role of numerical models in uncovering the often-hidden mechanisms that influence droplet motion.

Practical considerations also support the use of numerical simulations in design and manufacturing of superhydrophobic surfaces. Simulations can reduce design costs and accelerate the development period, minimizing the need for iterative experimental trials. Efficient and accurate simulations can identify surface properties such as roughness and contact angles, and suggest improvements. These insights are crucial for fine-tuning surface designs[22] for applications ranging from anti-icing to self-cleaning. By studying the fundamentals of the interaction of droplets with each other or with other particles deposited on a surface, the simulations provide a possibility to understand the dynamical interaction of the droplets at the early-stage of self-cleaning up to their eventual detachment from a surface.

Numerical analysis can also estimate the behavior of agglomerates in humid or dry surroundings and their possible return to the surface. There is also a possibility of heat-transfer studies in such processes[23], [24], which can be beneficial to improve the behavior of dropwise condensation, but such studies have not been the scope of this project. As a result, the ability to in-

clude such physics in a numerical analysis allows for understanding of wetting behavior, that has been triggered by local effects at micro-scales, in comparison to experimental studies that mostly depend on the general outcomes of particle removal and measurements of heat transfer rates. However, despite the mentioned advantages, numerical models still possess innate and early-development challenges, particularly in terms of assumptions and boundary conditions that may not always reflect the real-world behaviors. Many current models rely on simplified representations of dynamic contact angle behavior, surface roughness, capillary forces and interfacial numerics. These limitations call for a continued development and validation of numerical models to ensure their accuracy and applicability.

Therefore, numerical studies have a lot of advantages but the currently implemented models are often limited to certain applications or include an extensive list of assumptions. This thesis aims at contributing to this ongoing development by proposing novel models and approaches for wetting analysis and capillary effects, specifically tailored to applications involving superhydrophobic surfaces. In particular, we focus on improving the representation of dynamic contact angles[16] and including correct adhesive physics both between a droplet and a substrate and a droplet and a captured contaminant, areas where current models lack consistency. Additionally, the simulation framework was validated against experimental data to ensure that the findings are both accurate and practically relevant. Development of new models, validation procedures and critical thinking in the assumptions that the study can afford, has helped to acquire accurate and pinpoint information with simulations. This thesis considers the development of new models for wetting analysis and capillary effects and the validation of important simulation settings, as one of the key contributions to the field.

1.3 List of studies of thesis

This thesis had a gradual increase in complexity, with utmost target to create a trustworthy framework that is able to study dynamics of droplets, wetting of superhydrophobic surfaces and capturing of dirt (contaminant) particles by droplets forming colloids.

i. The first study focuses on the hydrodynamics fundamentals that govern the coalescence of two equally sized droplets and the subsequent jump-

ing droplet phenomenon. It is investigated at different scales the effect of hydrodynamic physics, specifying the dominant dynamics, that drive coalescence dynamics. It is evaluated how the presence of a superhydrophobic surface influences coalescence, whereas a computational framework is developed, able to recover all the core principals for the fluids (liquid and gas).

In particular, the study focused on the accurate modeling of the interface transport phenomena, while maintaining a sharp interface and providing a trustworthy representation of its curvature, which is a crucial parameter when calculating the surface tension force. Moreover, it compared the validity of a constant normalized velocity under the theory of capillary-inertial regime and identified the scales for which deviations are observed. The study revealed the critical role of surface tension and droplet size in determining the efficiency of droplet jumping, laying the groundwork for further investigations.

ii. The next phase involved the effects of dissipation, often caused by pinning, which in a fluid dynamics study is noticed by the contact angle hysteresis under dynamical motion of the contact line on a solid surface. By studying how contact-angle hysteresis modeling influences droplet jumping, significant understanding of its restrictive nature was obtained. Hysteresis, the dependence of the contact angle on the history of the droplet's movement, was quantified in order to understand its impact on the jumping behavior. The research demonstrated that hysteresis can significantly affect the contact angle behavior, influencing the energy required for a droplet to jump. This finding highlighted the importance of accurately modeling hysteresis in simulations to predict actual behaviors of superhydrophobic surfaces in the jumping droplet sequences.

iii. In the third part of the project, a fully resolved particle was introduced in the domain. The purpose was to investigate for the first time a particle being captured by a single droplet as it was first reported by Yan et al.[25]. In this process, a droplet spreads and captures a hydrophilic particle, while due to its generated motion and displacement, it interacts with the superhydrophobic surface and the particle-droplet jumping is achieved.

The development work for the framework focused on producing a trustworthy particle behavior, by introducing and validating an adhesive, cap-

illary force. Moreover, the immersed boundary method was used to model the particle surface, and the rigid-body dynamics equations were coupled in the solver to account for its motion. The results were successfully compared with the mentioned experimental study.

A series of parameter studies were performed by varying properties of the droplet, substrate and the particle. With the numerical study that followed, a temporal evolution of the energy budget of the system was provided. The results of the parameter studies highlighted how contact angles contribute to energy dissipation and how the particle-to-droplet size ratio impacts the jumping velocity.

iv. The final phase of this thesis examined the mechanism of particle-droplet jumping by extending the framework to accommodate a surface textured with pillar-shaped structures. The results from the previous numerical work with the modeled smooth superhydrophobic surface were compared to those using patterned surfaces, for which reported jumping. In addition, the influence of textured surfaces was investigated, with a series of different pillar configurations and dimensions. The effect of the presence of pillars was also studied for different pillar contact angles.

   The findings revealed that higher pillars promoted more efficient jumping by reducing the dissipation due to a decreased substrate contact during oscillations. Additionally, the study showed that wider pillars increased the contact area and dissipation, thereby reducing the jumping velocity. Larger spacings between pillars favored the Cassie-Baxter state and promoted droplet detachment, while lower contact angles suggested the Wenzel state of wetting, with flooding of valleys.

1.4 Structure of the thesis

The structure of this document goes as follows. First, in Chapter 2 the thesis provides the theoretical background that is required to understand its aims and main targets. An analysis of superhydrophobic surfaces is provided, focusing on their wetting properties and advantages, and highlighting the main mechanisms that facilitate the process of self-cleaning. In the next sections, it is given the background regarding the two main self-cleaning mechanisms that this thesis deals with, the jumping droplets phenomenon and the one

that involves removal of a particle by a single droplet. The main objectives are stated in the last section of Chapter 2, with an emphasis on the scope of the work and how the numerical studies were designed and carried out in order to accomplish the thesis' objectives.

The numerical methods are explained in Chapter 3 by mentioning all the models that were included in the multipurpose framework developed for studying of self-cleaning studies from superhydrophobic surfaces. In Chapter 4, selected results are offered from the list of papers that are included in the thesis. This selection has been made with regards to the main findings of each study and how each of them fulfills the main objectives. The thesis finishes with a summary of the main conclusions of the included papers, reaffirming that the study's objectives have been met.

CHAPTER 2

Background

2.1 Superhydrophobic surfaces

2.1.1 Biological surfaces

Superhydrophobic surfaces are commonly found in nature. Many times in biology studies, scientists are fascinated by the performance of certain biological organisms with surfaces that excel in water-repellency and remain clean benefiting from different mechanisms of self-cleaning. This extreme hydrophobic behavior, from the old greek words "hydor"-water and "phobia"-fear, that of a superhydrophobic surface, is based on the ability to efficiently dewet the surface either by motion, shedding, gravity or other forms and minimizing the area of contact between liquid and solid[1]. In order to develop this characterization, natural surfaces have undergone many stages of evolutions. One example comes from the lotus plant, since the lotus leaf shows removal of dirt particles by droplets, taking advantage of the micron-size structures that have developed on the upper surface of the leaf. This behavior has been termed the lotus effect.[26], [27]

Some insects that carry large wings in relation to their body need neat

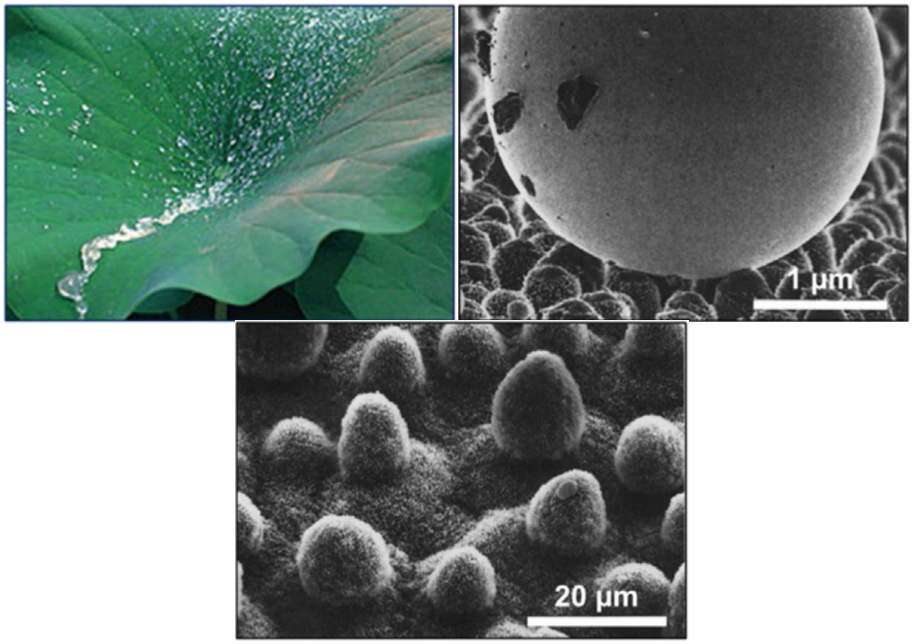

Figure 2.1: The lotus leaf (top-left) and the structure of its superhydrophobic surface(bottom). The droplet(top-right) captures dirt particles before removing them, Ref.[26].

surfaces, clean from dirt particles or microorganisms that can deteriorate the wings performance. A nice example is the cicada wings, which has been described in the literature multiple times for its ability to remove contaminants[6], making use even of the jumping droplets phenomenon, see Section 2.2. The two-layer structure of the surface with features of both micron- and nano-size has been suggested to be key behind its unique abilities[28]. By studying such surfaces, scientists try to create similar roughness patterns for applications that require superhydrophobicity[29]. Such studies belong to the category of biomimetics, as they mimic the biological surfaces to create artificial ones, for technological purposes.

Figure 2.2: Depiction of contact angle at the contact line location, highlighting the stresses of Young-Laplace equation at contact line $\gamma \cos\theta = \gamma_{SA} - \gamma_{SL}$, Ref.[22].

2.1.2 Surface wetting theory

The theory of surface wetting explains how liquids interact with solid surfaces. Key concepts include the contact angle (Fig. 2.2), which measures the wettability of a surface. Superhydrophobic surfaces exhibit high contact angles, typically greater than 150 degrees, indicating that water droplets form nearly spherical shapes and have a minimal contact with the surface[18]. The Young-Laplace equation describes the balance of forces at the contact line for a flat surface[22]. In a dynamic motion of the contact line, the adhesive forces may vary and fluctuate, while an apparent deformation of the contact angle is noted, which is then termed a dynamic contact angle[30]. In such situations, the description of the instantaneous forces with analytical formulations becomes more complex, and models have been devised to connect the continuum properties with the deformation characteristics.

However, deformation also takes place at a static wetting, in occasions when the liquid is under stresses. The stresses will deform the curvature of the interface near the contact line, causing a variation of the apparent contact angle[31]. Before motion is to be initiated from the stresses, a pinning behavior of the contact line is noticed, which exists in both an advancing or a receding tendency to move the contact line[32]. The pinning can be caused by surface roughness or heterogeneities and it literally suggests that the contact line will not move regardless of the deformation of the interface curvature close to the solid[1], [33]. The difference between the two limit contact angles, advancing and receding, as registered before motion of the droplet would occur, is called the contact angle hysteresis[14].

The contact angle hysteresis is a measure of energy dissipation, as the provided energy will be partly absorbed in the pinning behavior. Only a part of that energy will return when the fluid stops applying stresses near the contact line and the interface relaxes from the limit advancing or receding angle. Superhydrophobic surfaces typically show a reduced contact angle hysteresis when compared with conventional ones, either hydrophilic or hydrophobic. Studies have focused on minimizing as much as possible this dissipative in-

fluence by manufacturing surfaces with a limited contact angle hysteresis[34]. Similarly, the sliding angle is another measurement for hysteresis, by measuring an angle at which a droplet initiates movement on a tilted surface. Typically, surfaces made of materials that promote low surface energy can exhibit extreme superhydrophobicity and low hysteresis or sliding angle[35].

2.1.3 Types of surfaces and how are they manufactured

Most attempts to achieve superhydrophobicity have focused on the use of elongated structures, often rectangular or cylindrical pillars with flat top surfaces[36], that create voids between them. As confirmed from the biological superhydrophobic surfaces, the liquid wets the top of the pillars and creates a liquid meniscus between the structures, leaving a region of air-pockets in the cavities between the pillars[37], [38]. As a result, this facilitates water-repellency and high contact angles. The behavior of wetting micro-structured patterns is based on the theory developed by Cassie and Baxter [39], which measures the contact angle for a sessile droplet as a function of the wetted area, the actual total solid area and the intrinsic contact angle in the absolute vicinity of the surface (nano-scale). The distance between pillars, also called the pitch, is another significant factor to achieve the state where a liquid droplet is solely suspended to the pillars' tops. Moreover, the ratio of the wetted area to the total solid area and the width of the pillars influence the wetting regime[33]. In case of wide pillars and small pitches, it is challenging to sustain the Cassie-Baxter state and this would cause partial or full wetting of the side and the bottom of the pillars, two states that are called the partial-Wenzel and Wenzel states, respectively[22].

Studies have focused on optimizing the connection between the dimensions of textured patters and a superhydrophobic wetting. However, further improvement was achieved with a second layer of nanoscale hair-like features, similar to what was observed in the lotus leaf, which was enabled by specific treatments[29]. This layer increases the intrinsic hydrophobicity and enhances the superhydrophobic performance of textured surfaces. Studies have specifically linked the presence of such a nanostructured layer to a reduced contact angle hysteresis, which promotes improved liquid mobility on the surface[40]. Consequently, several advanced manufacturing techniques have successfully achieved extreme superhydrophobicity by incorporating nanoscale treatments. For example, Yan et al. [41] demonstrated that such nano-treated surfaces

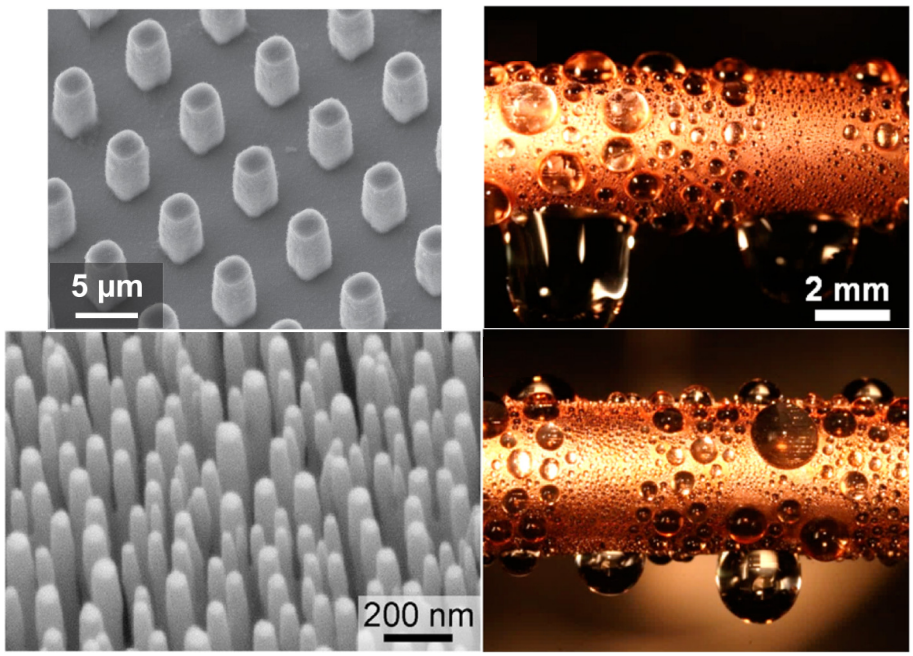

Figure 2.3: Two examples of manufactured microstructures with pillars that are used for improved drop-wise condensation by Ref.[42](top-right) and Ref.[43](bottom-right). Two instants of drop-wise condensation are shown on a superhydrophobic surface of copper coated with graphene at Ref.[44].

exhibit significantly enhanced water-repellent properties, outperforming two-tier treatment with micro-structures, opening new possibilities for practical applications in self-cleaning and anti-fouling technologies.

In the manufacturing process, two types of surfaces can be highlighted. The one would be surfaces that can be manufactured in a textured and precise manner that controls the shape and distance of the micro-structures (structures with dimensions from 0.5 µm and greater)[29], while the second one is with coated surfaces designed to create random directions of the structures, with multiple asymmetric points of contacts and different heights between structures. Such a design also causes the normal direction to the solid to vary across the surface and enables cases with wetting gradients and capillarity in-

stabilities. Biological surfaces showcase such properties. On the other hand, manufactured surfaces with a precise deposition of micro-structures undergo reinforcement with an additional layer of random nano-structures with an intrinsic hydrophobic wettability[45]. The latter layer combined with the air-pockets between the micro-pillars aids to achieve a superhydrophobic behavior of these hierarchical surfaces.

From the perspective of incorporating superhydrophobic surfaces into numerical studies, a couple of previous studies opted to simulate the interaction of droplets with micro-structures using the actual shape of pillars with two-dimensional and three-dimensional analyses[46]. Depending on the dimensions of the pillars, the refinement of the domain of the fluids requires adjustments in order to properly capture the influence of the boundary geometry to the fluid. This thesis will initially evaluate studies that cannot fully resolve such features. A variety of simulation cases involving droplets on superhydrophobic surfaces will be performed with the droplet radii spanning from a few microns to up to 500 µm. The larger cases potentially require cell sizes that may be up to 100 times larger than the roughness of the surface. For the cells close to the contact line and aiming at with fully resolving boundary features, such a high resolution may interfere with the stress singularity problem that happens when the contact line moves on a no-slip boundary. Hence, within a continuum description, the presence of roughness (microstructures) is modeled with a slip effect, known as the Navier slip boundary condition, where the velocity is proportional to the local shear stresses of the fluid[30], [47], [48]. The slip factor is modeled as a length scale proportional to the grid resolution of the neighboring wall cells or otherwise the structures height[22]. The contact angle is implemented with a static value or with a dynamic contact angle model, that can be dependent on the flow properties. In the later stages of the thesis, the behavior of a smooth surface will be compared with the actual geometry of a pillared surface, for a case when the dimensions of the pillars exceed the dimensions of the cells in the domain.

2.1.4 Advantages and disadvantages of superhydrophobic surfaces

Among the many advantages of superhydrophobic surfaces, water-repellency and self-cleaning from contaminants are the two important features. In addition, improved efficiency for drop-wise condensation[49], directionality with

grooves[50] and a desired wetting gradient[36], [51], [52], defrosting and anti-icing[53], have been mentioned as other benefits of using superhydrophobic surfaces in technological applications.

On the other hand, an analysis of the practicality of superhydrophobic surfaces suggests that superhydrophobicity often degrades in time, with an increase in the contact-angle hysteresis and a decrease in the mean contact angles observed[29]. The current costly manufacturing procedures of innovative surfaces require treatments aiming at regenerating the desired wetting properties after a certain period. Studies have connected the rate of deterioration of the superhydrophobic quality with the exposed temperatures or the humidity levels[29]. Often the desired applications for superhydrophobic surfaces are in enclosed devices, such as in the case of condensing heat-exchangers[54], and resurfacing would be extremely hard to achieve practically, being both time-consuming (especially if it causes downtime) and costly.

With an improved and self-sustained self-cleaning quality, we aim in this study to suggest surface modifications that facilitate more efficient self-cleaning processes. In addition, we target to uncover the fundamental stages behind these processes. The goal is to advance the knowledge on self-cleaning surfaces, aiming at reducing manual and forced cleaning interventions. The efficient removal of contaminants and droplets will then increase the life-time of these surfaces.

2.1.5 Surface cleaning applications

In this part of the thesis we develop a framework to study specific behaviors of wetting phenomena involving superhydrophobic surfaces and droplets. Even though the subsequent studies will focus on two specific self-cleaning mechanisms, the jumping of only droplets and the jumping of a particle-droplet system, it is essential to recognize that the same framework will have the ability to capture physics within a wider range of configurations of fluid-solid interaction that facilitate the cleaning of the substrate. Following, a list of these mechanisms involving superhydrophobic surfaces is presented. The author considers crucial to emphasize that with the use of the developed framework, research on optimizing superhydrophobic surfaces can be tailored to a corresponding application. An advantage of these simulations is the ability to

combine multiple mechanisms and to quantify their respective efficiencies.

Lotus effect

- Superhydrophobic surfaces can achieve self cleaning by harnessing the lotus effect, where particles are captured and removed by droplets shedding on the surface due to gravity or forced droplet exposure like to a rainfall. Since high contact angles are acting, the droplet shows limited pinning forces and low adhesion energy, and it efficiently rolls off or slides away from the solid surface.[26]

Jumping droplets

- Jumping droplets by a spontaneous coalescence of two or more droplets is another self cleaning mechanism, which will be explained in detail in Section 2.2.

Electrostatic repulsion

- Contaminants (particles) are subjected to electrostatic charges, which repel them and lower their adhesive properties[55], [56]. Existence of stationary or moving droplets would facilitate the particle removal, therefore these scenarios have scientific interest. Hydromagnetics should be considered for this setup.

Grooves removal

- Droplets and liquid films can be influenced by the existance of grooves between microstructures of the substrate. These grooves possess anisotropic wetting properties that help guide the liquid to a specific direction, carrying it away for collection or other purposes[50], [57]. In case of condensation, condensed microscale droplets can start shedding, sweeping a number of other droplets in their path, following a series of coalescence events along the microgrooves and the eventual dewetting[58].

Surface Vibrations

- With elastic vibrations or oscillatory rigid-body motion of the surface, particles and droplets can be removed from a substrate with their acquired momentum. The contaminants need to overcome the adhesive

forces acting on them, and depending on the nature of adhesion, a combination of different cleaning mechanisms may be required to overcome adhesion for their eventual removal[6].

Air Shear Cleaning

- Shear flow is considered a typical method for cleaning surfaces. In the existence of a superhydrophobic surface, the minimal work of adhesion that is required to remove droplets can set them in motion with shear flow, facilitating dirt particles removal or even droplet jumping perpendicular to the surface[59]. In the case with roughness at the scale of a few micrometers, the shear flow should influence neither the structure of the surface pattern nor their nano-coated treatment that enables hierarchical wetting properties.

2.2 Droplet coalescence and jumping

Droplets coalescing and jumping became the topic of extensive research due to the ability of the droplets to self-remove from the surface without the use of external energy[60], [61]. The kinetic energy that was recovered during coalescence is the aftermath of the released surface energy, coming from the difference in surface energy of the two initial spherical droplets and the final settled spherical merged droplet. A high curvature, present at the location where coalescence initiates, causes the creation and the subsequent rapid expansion of a liquid bridge. This creates oscillation waves transversing through the droplets interface. The inertial expansion of the liquid bridge initiates the point of contact with the substrate and the expansion of the contact area with the superhydrophobic surface stores energy which is recovered by the droplet during its upwards momentum. Most of the upwards momentum energy is gained through interaction of the liquid bridge hitting the substrate and subsequent shape oscillations that expand the merged droplet in the vertical direction, before it eventually retracts and jumps from the surface[4], [61]–[64].

For a numerical study, to accurately capture the removal of particles, it is needed to develop a trustworthy framework that is able to recover the droplets jumping scenario and to deepen the understanding of different stages of that process, in full detail and at the smallest hydrodynamic scales. Therefore, the

surface tension force, contact line stresses, curvature handling and interface sharpness and transport should be controlled by the framework in a trustworthy manner and for all the relevant temporal and spatial scales. We initiate the study from a point that the hydrodynamics is properly captured. We follow by focusing on the interaction of the interface and the solid at the location of the contact line. In this topic, the thesis pays close attention to the contact-angle influence and the existence of pinning and the degree of hysteresis. The exact contact angle value at the advancing or receding motions of the contact line needs to be controlled by the framework and the effect should be validated and quantified to master the interaction of the droplets and a superhydrophobic surface using a continuum description. Therefore, with simulations we aim at recovering with accuracy the stages through which the process goes.

The jumping droplets was reported initially by Boreyko and Chen[60]. When a liquid condensates, the formed droplets coalesce and then spontaneously depart from the superhydrophobic surface. By studying the behavior of the merged droplets of different sizes, the authors reveal the connection between the relevant mechanisms of the process and the capillary and inertial forces, suggesting that viscosity is not the main reason for dissipation. In the same study they showed how the jumping velocity follows the capillary-inertial scaling, based on the time and velocity scales of the capillary-inertial regime.

Subsequent studies defined the efficiency of the jumping motion as a percentage of the released surface energy[61]. Either using experimental[34], [42], [52], [65] or numerical analyses[59], [66]–[73], researchers reported the main stages of the process, estimated the influence of the surface wettability and roughness structures, understood the importance of size matching for the droplets and located the cut-off regions[67] in the smallest and larger length scales where the capillary-inertial scaling occurs.

It is essential for a numerical study, such as the one carried out in this work, to assure the validity of interface transport modeling. The simulations require accurate calculation of the curvature at every time step. Due to the Laplace pressure, spurious currents can arise from artificial velocities induced at the interface[74]. Such errors are even more pronounced at the micrometer scales due to the strong surface tension.

From the numerical perspective, it has been a challenge to resolve the evolution of all stages of the jumping process, which is even more difficult at the smallest length-scales. At a specific length scale, the competing interaction of

the surface tension and inertial forces dictate the time scales (the capillary-inertial time scale t_{CI}) during wetting and coalescence, which is additionally dependent on the fluid properties. The coalescence dynamics and the liquid bridge expansion are governed by the identified time scales, which in turn define the instance of the maximum expansion point. The time scales decrease with a power of 1.5 following a decrease in the radius of the droplet. This suggests that experimentally capturing the jumping process at the scale of a few microns becomes next to impossible.

The eventual normalized jumping velocity is presented as the ratio of the jumping velocity and the capillary-inertial velocity scale U_{CI} of the system. The capillary-inertial velocity scales with the initial radius of the droplets with a power of -0.5. To follow a capillary-inertial scaling, the normalized velocities are required to be constant and the jumping velocity needs to scale one to one with U_{CI}. Therefore, when the radius decreases the real jumping velocity increases exponentially. In their study, Boreyko and Chen[60] expanded on this relation and pointed the existence of a cut-off radius, under which the droplets-substrate interaction is not solely governed by the surface tension, inertia and the capillarity-induced wetting forces. At the length scales (i.e. droplet radius) below $R_i \leq 25$ µm, the jumping efficiency drops and the identified scaling law breaks down. Later, this finding was validated from the mentioned studies, even though different values for the cut-off radius were reported[66], [67]. Further details are also offered in the introduction section of Paper B. Above the cut-off radius, the non-dimensional jumping velocity has been computed around 0.20 – 0.26[34], [45], [61], [64], [69], [72], [75]–[82].

A limited number of studies studied the cause of the cut-off behavior. We exemplify the numerical work of Attazardeh and Dolatabadi[66], which introduced rectangular pillars beneath jumping droplets, and suggested that the ratio of the characteristic dimension of the pillars and the radius of the droplets is an important parameter. This numerical study concluded that the interaction with the sides of micro-structures affected the energy dissipation. Assuming this is a major effect, it is pointed out that the cut-off radius becomes dependent on the dimensions of the pillars for the surfaces having textured patterns, as well as on the distance between pillars.

The Ohnesorge number Oh compares the viscous forces to the combination of the inertial and surface tension forces. Since its definition makes that number inversely proportional to the radius of the droplets, it increases when

the droplets become smaller. Experimental and a couple of numerical studies mentioned ejection of coalescing droplets for sizes as small as $R = 0.5$ μm[51], [52], [81], [83]. Therefore, the droplets with a high Ohnesorge number are considered capable to overcome the viscous dissipation of the fluid. However, viscous effects that are attributed to the contact line behavior are less straightforward to estimate theoretically for a dynamic case and they can only be modeled within a continuum framework if a suitable dynamic contact angle model is in place, or if the geometrical features are well resolved. Nevertheless, in the latter case, the study needs to account for the stresses singularity at the location of the contact line, which predicts infinite stresses while the interface is in contact to the solid and a no-slip behavior is considered. This has been ameliorated in multiple studies by the existence of a slip boundary condition. The Navier slip implementation has been often introduced for modeling patterned superhydrophobic surfaces as a flat surface, but different slip length values have been implemented. In a more popular approach, the slip length has been connected to the smallest cell size in the domain of interest[84]. Other studies promote a slip length that relates to the height dimensions of surface structures, modeling the presence of a gas as air pockets beneath the liquid[22]. In that case, the boundary is considered to have a flat geometry for the numerical studies.

2.3 Particle-droplet coalescence and jumping

Droplet coalescence and jumping has been a topic for extensive numerical and experimental studies, with main interest to study the fundamental physical phenomena that govern the process. On the other hand, when a particle is involved, the complexity increases. From an experimental side, a limited number of works that published on this subject faced difficulties to study all relevant spatial scales and to identify the underlying phenomena. In particular, it is not straightforward to separate the effect of a droplet-substrate contact from that of a droplet-particle contact, and to define and quantify the energy losses that are attributed to either of the interactions.

Of particular interest are the studies that suggested removal of particles harnessing the jumping droplet phenomenon. Wisdom et al.[6] described that the droplets can capture the contaminants under the following three circumstances. First, a behavior of floating was observed, where a droplet that has

entrained a solid particle, fully wetted by the droplet, coalesces with another droplet and initiates a jumping reaction. The second form was termed as lifting and includes a particle that is captured at the interface of a droplet before coalescence or that the particle is captured by the interface of an oscillating merged droplet following coalescence. The third mechanism suggested the existence of an aggregate of particles, acting as a colloid after being wetted by a liquid droplet and promoting the formation of liquid bridges between particles. When two such agglomerates come into contact, the creation of a large liquid bridge can initiate motion that causes jumping.

In a numerical study by Farokhirad and Lee[85] the authors studied the removal of a spherical particle by jumping droplets. To decrease complexity in the study the particle was already encapsulated by one of the droplets. It is important to highlight that the capillary forces that attract a solid body to a liquid cannot be neglected at the micrometer scales, where the capillary forces are significant in relation to the hydrodynamic stresses. The mentioned work considered a model that was developed for implementation for a Lattice-Boltzmann fluid dynamics solver, which had been earlier validated for different cases. The studies for the validation of the adhesion model from earlier work[86] were limited, and the particle-droplet study did not expand regarding possible spontaneous wetting phenomena in the case of jumping droplets.

In another work, Yan et al.[25] for first time pointed out the existence of a passive self-cleaning mechanism of a jumping particle-droplet. In the presence of a superhydrophobic surface, a sessile droplet initiates spreading on a spherical solid particle with hydrophilic wettability. The liquid bridge created from the spreading process expands, as the liquid front at the point of the contact line is spreading over the particle surface. The inertial motion of the formed liquid bridge, followed by oscillations in the shape of the droplet, and displacement of the spreading liquid towards the direction of the particulate sphere, causes contact of the liquid bridge front with the substrate and expansion of the contact area. As a result, the droplet interacts with the substrate and an upwards motion follows. During particle wetting, the droplet reaches maximum expansion area on the particle. The capillary forces acting at the contact line are responsible for the adhesion of the particle on the interface of the droplet. As an aggregate, the particle-droplet system detaches from the substrate, overcoming gravitational forces. It then performs travels through

the air and a rotation around the center of mass of the system may also appear.

Specific complex details from the mechanism still lack characterization and it is considered that numerical simulations are required to succeed in quantifying the contact line physics or the dynamic oscillations of the droplet, which is caused by the spreading motion on the particle and the impingement of the spreading liquid front on the superhydrophobic surface. The novelty of this task is highlighted by the absence of other numerical studies and the previously mentioned challenges in modeling the interaction of the interface with the particle. The models developed must address the contact line's movement on the superhydrophobic surface, droplet spreading on a curved particle surface, and the very small temporal and spatial scales governed by the fluid and particle properties.

In this study, the numerical modeling was selected with intention to handle general moving solid bodies, such as a spherical particle. The immersed boundary method (IBM) approach was opted, since it can model the location of moving boundaries and generic geometrical shapes. Both the superhydrophobic surface and the particle were modeled under this method, using a structured mesh for the domain, which incorporated adaptive mesh refinement (AMR) to refine locations such as the solid boundary or the interface, where we require finer resolution. The IBM is capable of computing the fluid hydrodynamic forces on the bodies' surfaces on the triangulated surface meshes of the immersed body. In conclusion, the thesis tries to emphasize in the limited knowledge that was available regarding the particle-droplet jumping mechanism, prior of the work performed in the two latter papers that are included in the thesis.

2.4 Thesis objectives and aims of the research work

- **Characterize properties of superhydrophobic surfaces and explore their design for self-cleaning purposes.**
- **Identify processes of mechanisms of droplets:**
  i. during wetting superhydrophobic surfaces,
  ii. during coalescence,

iii. during spontaneous spreading on curved surfaces.

- **Develop a comprehensive framework handling complex interactions of droplets, particles and surfaces.**

In this thesis, it is considered as main target in this study to bring further knowledge on properties of superhydrophobic surfaces in de-wetting situations that facilitate self-cleaning. The value of such work would be to suggest new designs or to provide characterization of designs that are currently used in various applications. To develop on that, the project has been broken down to two further objectives that will eventually guide us to the main aim of this study.

For the thesis, as the second objective, it is specified the need to enhance the current knowledge on several mechanisms that can occur in the presence of droplets smaller than the capillary length and that belong to the region where capillary and inertial forces are dominant. The third objective then becomes the need for a numerical framework that will be able to capture all the details of the processes that occur in these mechanisms, with a sufficient time- and spatial-resolution.

Within the self-cleaning mechanisms where only droplets are involved, it is isolated in Paper A the droplet coalescence and then the simplified modeling of wetting contact angles as processes that need to be understood. A study of the jumping velocity and energy efficiency in the topic of jumping droplets has been performed in that regard. In Paper B, a detailed study related to advanced contact-angle models, for the mechanism of jumping droplets, was undertaken with an outlook to characterize the wetting behavior of superhydrophobic surfaces with regard to effective contact angle hysteresis.

Paper C had two connections with the three main objectives. First, the inclusion of a particle required additional models to handle the relevant physics at the continuum scale. However, the study also analyzed i) the unique mechanism of particle-droplet jumping involving a single droplet and ii) the spreading dynamics of a droplet on a spherical surface of a hydrophilic particle within the capillary-inertial dominated scales. We consider the latter process to be of particular interest and therefore the spreading rate factor was evaluated to estimate the gained inertial kinetic energy in the system. Therefore, more processes of self-cleaning mechanisms were identified, and we were able to enhance the current numerical models within the framework with the development of a model for capillary forces on solids, that was validated for the

process.

The last study of Paper D focused on understanding the interaction of a droplet with a microstructured superhydrophobic surface during the particle-droplet jumping mechanism. Pillars were introduced within the numerical framework and studied their dynamic wetting and de-wetting during jumping. With the findings obtained in Paper D, an analysis of different pillared patterns on superhydrophobic was presented, that offered clear directions for designing superhydrophobic surfaces having an improved jumping efficiency.

CHAPTER 3

Methods

The numerical framework had to be developed in steps and validation was required when additional models were introduced. The basis of the software was a finite volume solver of the principal fluid dynamics equations that describe the motion of fluids as continuum, solving for the conservation of mass and momentum in the cells of the discretized domain. The equations for an incompressible case write as:

$$\nabla \cdot \mathbf{v} = 0\,,$$
$$\frac{\partial (\rho \mathbf{v})}{\partial t} + \mathbf{v} \cdot \nabla (\rho \mathbf{v}) = -\nabla p + \nabla \cdot (\mu \nabla \mathbf{v}) + \rho\, \mathbf{g} + \mathbf{f}_{SF}\,, \tag{3.1}$$

with $\mathbf{v}$ being the velocity vector, P is the pressure, ρ is the density of the cell, μ is the dynamic viscosity and $\mathbf{g}$ is the gravitational acceleration. The body force $\mathbf{f}_{SF}$ per unit volume is the force caused by the surface tension, acting at the location of an interface of two fluid phases and normal to it.

The existence of a sharp-interface is handled with the method of **volume-of-fluid** (**VOF**). This method belongs to the general category single-fluid equation, sharp-interface methods for multiphase flows and it uses a color function to prescribe the location of the phases. The color function is updated

with a transport equation that only advects it to obtain the new interface position. This model is often used instead of other direct numerical simulation (DNS) methods such as the following:

1) the **level-set method**, that obtains the interface with a smoothed Heaviside function and advects it with artificial diffusion,

2) the **phase-field method**, which is a diffuse-interface method that solves the Cahn-Hilliard equation with the chemical potential between the phases to provide the forces at the interface,

3) the **front-tracking method**, where the interface is a surface mesh with langrangian markers and may require intervention steps to mitigate surface mesh distortion.

These multiphase models have also been used as a combination of two models. In this work, the preference to the VOF approach was based on the simplicity of the implementation, the strong sharpness of the interface and the absence of diffusive behavior of the two phases. In order to assure that VOF accurately represent the interface motion, special attention is required to the convective process of the transport equation, the face velocities for the cell faces that are occupied with different phases, and the time- and spatial discretization to assure fully resolved interface and a well computed curvature at each time-step.

In the color function equation for VOF, the solver computes the volume fraction field with the following transport equation:

$$\frac{\partial \alpha}{\partial t} + \mathbf{v} \cdot \nabla \alpha = 0 \,, \tag{3.2}$$

where α is the volume fraction chosen to be the color function. It is needed to emphasize that in another approach, a compressive term is used to mitigate numerical diffusion. However, in the implementation of the software, a smoothened volume fraction gradient is used, as by Brackbill et al.[87], to estimate the curvature κ with better accuracy, especially for highly distorted interfaces. This technique refines the volume fraction gradient by applying a series of Laplacian filters to the volume fraction field[74]. The approach that uses the gradient of the volume fraction to get κ has been also part of the original continuum surface force (CSF) method [87], which uses the body

force $\mathbf{f}_{SF}$ in the momentum equations, calculated as:

$$\mathbf{f}_{SF} = \sigma \kappa \mathbf{n}\,, \tag{3.3}$$

where σ is the surface tension between of the interface and $\mathbf{n}$ is the normal vector at the interface.

For the computations of the next time-step, the fluid properties are given by volume averaging using the updated interface location:

$$\rho = \alpha\,\rho_1 + (1-\alpha)\,\rho_2\,, \tag{3.4}$$

$$\mu = \alpha\,\mu_1 + (1-\alpha)\,\mu_2\,, \tag{3.5}$$

where the sub-indices represent the two different phases.

To compute κ the equation uses the divergence of the normal vector to the interface as:

$$\kappa = -\nabla \cdot \hat{\mathbf{n}}\,, \tag{3.6}$$

with $\hat{\mathbf{n}}$ being the unit vector normal to the interface, which is computed from the volume fraction respectively:

$$\hat{\mathbf{n}} = \frac{\mathbf{n}}{\|\mathbf{n}\|} = \frac{\nabla\alpha}{\|\nabla\alpha\|}\,. \tag{3.7}$$

The transport equation contains only a convective term, but a couple of advanced models are required to obtain the optimum transport behavior of the interface. First, there was focus on the calculation of the velocities on the faces. The Rhie-Chow[88] model uses a higher order interpolation of the pressure field, to give an estimation of the velocity variation across the face of the cell, as a result of the pressure gradient at the face. Similarly, the balanced-force method[89] is interpolating with regards to the surface tension force $\mathbf{f}_{SF}$ to get a better velocity at the interface. Moreover, the convective scheme selected for the discretization of the volume fraction equation is the fully compressive and bounded scheme CICSAM (compressive interface capturing scheme for arbitrary meshes) to get the volume fraction at the face, as a function of the volume fraction at the faces. The scheme compares the velocity normal at the interface, the angle between the local velocity and the normal vector to the interface and the Courant number (CFL), which compares the transport per timestep with the cell size. The boundedness of CICSAM is

further enhanced by restricting CFL < 0.5.

The linear system of equations is solved in a segregated manner according to the SIMPLEC method[90] for coupling between the equations, solving for the velocity components and the pressure in a co-located grid. In the adaptive mesh refinement, the mesh obtains a cubic form and problems of mesh quality are avoided.

As mentioned in section 2.2 a slip velocity is given at the boundary for the superhydrophobic surface, which is modeled with the Navier slip boundary condition. The slip velocity v_{slip} is obtained from:

$$v_{slip} = \lambda_{slip} \left. \frac{dv}{d\mathbf{n}_{\mathrm{w}}} \right|_{\mathrm{wall}} , \tag{3.8}$$

where $\mathbf{n}_{\mathrm{w}}$ represents the normal direction to the wall and λ_{slip} is the slip length between the stagnation point and the boundary.

To implement a contact angle that distinguishes between an advancing and receding motions of the contact line, the method provided in G ohl et al.[91] was used, referred to as quasi-static. It determines the apparent contact angle, implemented by editing the interface normal at the wall, with the static advancing or receding angle for the surface. It chooses based on whether the contact line velocity indicates advancing or receding motion.

A dynamic contact angle model was further used to model the hysteresis phenomena, caused by surface roughness or pinning of the contact line. The Kistler model was selected, that applies the Hoffman function f_{Hoff} [92], [93], which is a function obtained by correlation to experimental data. The initial value for static configuration is provided by the advancing θ_{adv} and receding θ_{rec} angles that are experimentally provided for each surface. A modification on the Hoffman function by Jiang et al.[94] that was specific for high contact angle surfaces has also been implemented. That study demonstrated that the Kistler dynamics contact angle model is able to capture the behavior of experimental data for hydrophobic and superhydrophobic surfaces. The equation reads

$$\theta_{dyn} = f_{Hoff} \left(Ca + f_{Hoff}^{-1}(\theta_{st}) \right) , \tag{3.9}$$

where $f_{Hoff}(x) =$

$$\cos^{-1}\left(1 - 2\tanh\left[5.16\left(\frac{x}{1+0.332x^{0.99}}\right)^{0.62}\right]\right). \tag{3.10}$$

The solids are modeled as immersed bodies in the eulerian domain and the immersed boundary method (IBM)[95] is implemented to resolve the surface location, impose the boundary conditions for the fluid at the solid surface and compute the forces of the fluids that act on the surface. The method that was used to set the boundaries is the mirroring immersed boundary method (MIBM), which is a second-order accurate in imposing the boundary. From the location of the interface, a mirrored point towards the fluid is used. The point is equal distance from the wall as the node on the side of the solid is to the surface, in the normal direction to the surface $\mathbf{n}_{\mathrm{dS}}$. The velocity of the fluid in the surrounding cells is interpolated in the mirrored point $\mathbf{v}_{\mathrm{ext}}$. Then the velocity on the ghost cell to the solid side is prescribed, following the equation which assumes constant velocity gradient at the surface and considers the velocity of the boundary to be given from the surface velocity of the body $\mathbf{v}_{\mathrm{IB}}$ for a no-slip boundary condition. The implementation of slip boundary requires the term $v_{slip}\,\hat{\mathbf{t}}_C$ from the slip velocity and tangential direction of the velocity of the contact line $\hat{\mathbf{t}}_C$. The equation that provides $\mathbf{v}_{ghost}$ is the following:

$$\frac{\mathbf{v}_{ext} + \mathbf{v}_{ghost}}{2} = \mathbf{v}_{IB} \; + \; v_{slip}\,\hat{\mathbf{t}}_C \;, \tag{3.11}$$

where $\hat{\mathbf{t}}_C$ is given by

$$\hat{\mathbf{t}}_C = \frac{\mathbf{v}_{ext} - (\mathbf{n}_{\mathrm{dS}} \cdot \mathbf{v}_{ext})\mathbf{n}_{\mathrm{dS}}}{\|\mathbf{v}_{ext} - (\mathbf{n}_{\mathrm{dS}} \cdot \mathbf{v}_{ext})\mathbf{n}_{\mathrm{dS}}\|} \;.$$

The method performs for each triangulated area of the solid surface an extrapolation for the pressure and the fluid shear stresses on the boundary using the values of the properties from the mirrored cell in the fluid side. Then the total hydrodynamic force $\mathbf{F}_{\mathrm{IB}}$ is provided from the following:

$$\mathbf{F}_{\mathrm{IB}} = \int_{A_{\mathrm{tr}}} \mathbf{t}_{\mathrm{dS}} \cdot \hat{\mathbf{n}}_{\mathrm{dS}}\, dS, \tag{3.12}$$

where the fluid stress tensor is given by:

$$\mathbf{t}_{\mathrm{dS}} = -p\, I + \mu \left(\nabla \mathbf{v} + (\nabla \mathbf{v})^{\mathrm{T}} \right) . \tag{3.13}$$

The torque to the body $\mathbf{T}_{\mathrm{IB}}$ is calculated by:

$$\mathbf{T}_{\mathrm{IB}} = \int_{A_{\mathrm{tr}}} r \times (\mathbf{t}_{\mathrm{dS}} \cdot \hat{\mathbf{n}}_{\mathrm{dS}})\, dS . \tag{3.14}$$

In the existence of an interface attached to the solid surface, which is the location of the contact line C_l, a capillary force $\mathbf{F}_{cap}$ is also acting towards the solid and enables the adhesion responsible for capturing particles at an interface. This thesis studies capturing spherical particles with a droplet at the capillary-inertial scales. The adhesive force that the droplet exerts on the particle results from the line force along the contact line with direction tangential to the surface[95], [96], as per the definition:

$$\mathbf{F}_{cap} = \int_{C_l} \sigma\, \hat{\mathbf{t}}_{int}\, dl , \tag{3.15}$$

with $\hat{\mathbf{t}}_{int}$ the unit vector tangential to the interface. It is given by

$$\hat{\mathbf{t}}_{int} = \frac{\hat{\mathbf{n}}_{dS} - (\hat{\mathbf{n}} \cdot \hat{\mathbf{n}}_{dS})\hat{\mathbf{n}}}{\|\hat{\mathbf{n}}_{dS} - (\hat{\mathbf{n}} \cdot \hat{\mathbf{n}}_{dS})\hat{\mathbf{n}}\|} . \tag{3.16}$$

In the work by Washino et al. [97], it was introduced a computational model, the continuum capillary force (CCF), to obtain $\mathbf{F}_{cap}$ on solid surfaces during the spreading of the gas–liquid interface. The approach inherits similarities to the CSF model used in VOF method [87], since the CCF model integrates the volume fraction gradient across each cell to specify the intersection between the interface location and the solid surface. The method returns a body force per volume of each cell $\mathbf{f}_{CCF}$ which subsequently sums for all the cells. By incorporating both the liquid-gas and solid-fluid interfaces, the model identifies the contact line based on the intersection of these interfaces, enabling precise capillary force calculations at this boundary.

In the CCF framework, the solid volume fraction field χ is utilized to achieve a gradual transition between phases, allowing for the calculation of the eulerian gradient across the solid surface. This gradient, in conjunction with two

Dirac delta functions for the liquid-gas and solid-fluid boundaries, estimates the line force along the contact line [97], [98]. The resulting force $\mathbf{f}_{CCF}$ for a cell containing the contact line is thus given by:

$$\mathbf{f}_{CCF} = \sigma \hat{\mathbf{t}}_{int}(\nabla\alpha \cdot \mathbf{t}_{C_l})(\nabla\chi \cdot \mathbf{n}_{dS}). \tag{3.17}$$

The tangential unit vector along the wall, projection of the interface normal to the wall is given by:

$$\hat{\mathbf{t}}_{C_l} = \frac{\hat{\mathbf{n}} - (\hat{\mathbf{n}}_{dS} \cdot \hat{\mathbf{n}})\hat{\mathbf{n}}_{dS}}{\|\hat{\mathbf{n}} - (\hat{\mathbf{n}}_{dS} \cdot \hat{\mathbf{n}})\hat{\mathbf{n}}_{dS}\|} \ . \tag{3.18}$$

The overall capillary force $\mathbf{F}_{CCF}$ and torque $\mathbf{T}_{CCF}$ are then determined by summing the cell contributions:

$$\mathbf{F}_{CCF} = \sum_{V_i} \mathbf{f}_{CCF}\, \Delta V_i \ , \tag{3.19}$$

$$\mathbf{T}_{CCF} = \sum_{V_i} (\mathbf{r}_{V_i} \times \mathbf{f}_{CCF})\, \Delta V_i \ , \tag{3.20}$$

where $\mathbf{r}_{V_i}$ represents the distance from the triangular solid surface's center at cell i to the rotation center of the particle.

For verification, we compare the CCF model against an analytical capillary force derived for a spherical particle and a stationary droplet partially wetting the particle. This force, representing the total line force integration around the contact line, is given by:

$$\mathbf{F}_{cap,\,ideal} = 2\pi\sigma R_p \sin a \cos\psi \ , \tag{3.21}$$

where R_p is the particle radius, a is the spreading angle from the particle center and ψ is the angle between the interface at the contact line and the direction of the centerline for the spherical particle and droplet $\hat{\boldsymbol{d}}$. From the geometry of the problem the method gets the angle as $\psi = \theta_{eq,p} + a - \pi/2$, with $\theta_{eq,p}$ being the equilibrium contact angle based on the mean of the particle's advancing and receding contact angles.

To approximate this ideal case' force, it was computed the direction of the force from the center of the particle to the droplet's mass center. The center of the droplet at a time instant was given by volume averaging. The magnitude

is based on the spreading angle a, computed by evaluating the liquid volume fraction at the periphery of the particle over a radial distance R_p from the particle center. The implementation checks over the periphery starting from the direction of vector $\hat{\boldsymbol{d}}$ and evaulating volume fraction of periphery points across a single plane. One horizontal and one vertical plane are used since the spreading can be assymetrical and a is given by the mean of the spreading angles in each plane.

We observed limitations in the CCF model under highly dynamic contact line conditions, where sudden retractions or advances at the particle surface affected $\mathbf{F}_{CCF}$ without capturing the physical peaks in attractive forces. To understand this, a comparison of the CCF model force to the analytical solution $\mathbf{F}_{cap,\,ideal}$ was performed. While directional behaviors were in agreement, the magnitude of CCF force exhibited stronger fluctuation and in cases showed inaccuracies between high and low values when compared to the result of the ideal case $\mathbf{F}_{cap,\,ideal}$. The magnitudes were also compared with the total hydrodynamic force calculated with IBM. Following the forces reaction to the hydrodynamic forces due to Laplace pressure inside the droplet, a modification to the magnitude of the capillary force is suggested from the mean of the CCF method and the analytical formula, such as $\|\mathbf{F}_{CCF,\,modif}\| = 0.5\,(\|\mathbf{F}_{CCF}\| + \|\mathbf{F}_{cap,\,ideal}\|)$.

A rigid-body dynamic solver is coupled to the solver to estimate the motion of the particle. An improved Euler time-stepping scheme is selected and coupling follows the Newmark method[99]. The stresses at each each face of the surface mesh for the solid particle are computed, to provide the correct force and torque contribution to the body. The particle motion is then obtained from the equations for translation and rotation:

$$m_{\mathrm{P}} \frac{d\mathbf{v}_{\mathrm{P}}}{dt} = \sum_{\mathrm{i}} F_{\mathrm{i}} = \mathbf{F}_{\mathrm{IB}} + \mathbf{F}_{\mathrm{CCF}} + \mathbf{F}_{\mathrm{gravity}} \ , \tag{3.22}$$

$$\mathbf{I} \frac{d\omega_{\mathrm{P}}}{dt} = \sum_{\mathrm{i}} T_i = \omega_P \times (\mathbf{I} \cdot \omega_P) \ . \tag{3.23}$$

It is noted that $\mathbf{I}$ stands for the moment of inertia of the particle. The framework was developed to accommodate non-spherical particles, but further studies on the influence and fundamental behavior of the capillary force $\mathbf{F}_{cap}$ will be required, in order to adopt particle jumping with generic particles under such dynamic wetting phenomena.

CHAPTER 4

Results Selection

Additional to the summary of the papers, offered in Section 1.3, a selection of results is provided here to facilitate the reading of the main outcomes in the current thesis and provide sufficient evidence for the conclusions.

4.1 Paper A

The first paper focused on investigating droplets with radius below 10 µm, or else mentioned as microdroplets, for the case of binary equal-sized jumping droplets. It compared the jumping mechanism with the jumping of larger droplets that belong to the capillary-inertial regime. The Ohnesorge number was used to make a qualitative comparison of the flow forces existing in each case. A simulation of droplets instantaneously coalescing, oscillating, spreading on a smoothed superhydrophobic surface and eventually jumping was performed, with a number of different sizes of as low as $R_{\mathrm{d}} = 0.5$ µm. This comparison is available in Figure 8 of Paper A or Figure 4.1 in the thesis. The results are presented in a logarithmic scale for the Ohnesorge number, with a second axis depicting their corresponding initial radius. The theoretical study of Boreyko et al.[60] suggested a constant jumping velocity in the

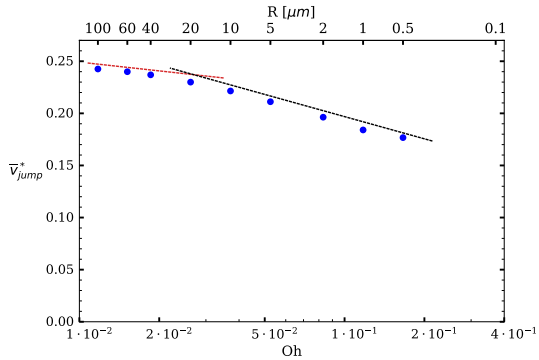

Figure 4.1: Jumping velocities v^*_{jump} normalized with U_{CL} at different droplet sizes and corresponding Ohnesorge number (log-scale). The red and black dashed lines represent the captured trends (i.e. different interpolation lines in log-scale) of jumping velocities from larger droplets and microdroplets.

non-dimensional capillary-inertial velocity scaling U. Instead we observed a slight decline in the velocity, which below the observed cut-off threshold it was reduced at a stronger rate. This is in contrast to experimental results by Enright et al.[83] that have used surface with micro-structures up to 0.8 µm and observed minimization of jumping velocity in the microdroplets. However, the numerical study included a smooth surface with static angles and hysteresis of up to 3°, therefore the actual interaction with roughness is considered a more significant factor for dissipation, in relation to pure hydrodynamic interaction of capillary, inertial and viscous forces. The jumping velocity results are accompanied by the evolution of the upwards velocity of the merged droplet for the size of 1 and 100 µm, to further emphasize the differences in the process, and showcase the ability of a microdroplet to undergo the same shape oscillation and dewetting process as the larger droplets of the capillary-inertial regime.

4.2 Paper B

Paper B developed on the established framework within Paper A and focused on the modeling of the interaction between droplet and superhydrophobic

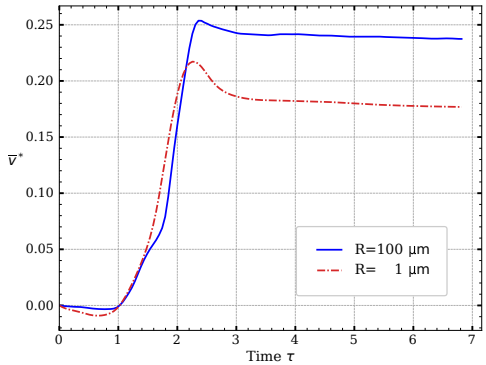

Figure 4.2: Time evolution of the upwards velocity for the droplets with $R_d = 100$ µm and $R_d = 1$ µm. Time and velocity are normalized with U_{CL}. The microdroplet reached reduced velocity and jumped at a later instant than the larger one.

surface. With benchmark experimental studies that studied superhydrophobic surfaces with evident hysteresis proper[29], [52], a validation and an 1-to-1 comparison with an ideal case that models no-hysteresis. The experimental values for the contact angles were $\theta_{adv} = 162°$ and $\theta_{rec} = 147°$, which accounts for a hysteresis of 15° in static situations. When the simulation models no-hysteresis, uses for contact angle the mean between the advancing and receding ones. The evolution of the upwards velocity for the two cases is provided in Figure 4.3. The size of both droplets in this comparison is $R_d = 25$ µm. Following the evolution of the jumping velocity a case with significant hysteresis gathers reduced upwards velocity and detaches at a later stage, withing a deceleration phase of the process. Therefore it has reduced jumping velocity and part of the droplet re-wets the surface before eventual jumping, with jumping velocity decreased by more than half of the velocity for a case that was modeled without hysteresis. In Paper B, a further depiction of instants for the two cases are provided with Figure 7 of Paper B. A number of additional studies were performed with various droplets' sizes, which analyzed the behavior of different equilibrium contact angles and different amount of hysteresis. Main outcome from these investigations were i) the delayed jumping and ii) the reduced jumping velocity for the cases with larger hysteresis at same sizes.

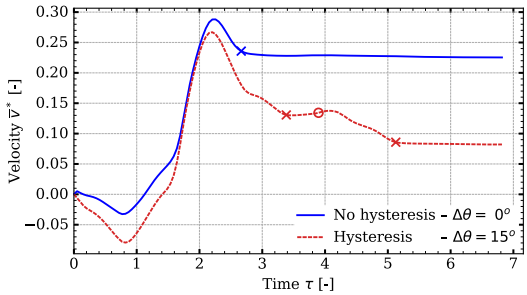

Figure 4.3: Time evolution of upwards velocity (normalized) for a case without and with hystereis. The the crosses (×) and circles (○) represent the moments where detachment and re-attachment occured correspondingly. It was observed a significant decrease for the jumping velocity, whereas a temporary re-attachment for the droplets with the hysteresis present is observed before jumping ultimately.

A dynamic contact angle allows for variations of the implemented angle with regards to the contact line velocity. The model of Kistler was selected to be compared with the static angles of the quasi-static method (see again Chapter 3). It would allow for further relaxation of the contact angle at high dynamic motions of the contact line. The inherited static hysteresis of the pinning phenomena was already accounted for within the simulation with the quasi-static values. In a dynamic case, were the interface gains speed, in advancing or receding motion, the model jumps between the two contact angles and introduces discontinuity for the normal vector field of the interface, between time-steps and cells. This is smoothened due to the series of cells introducing the contact angle value. In Figure 4.4, the jumping velocities, of cases with different contact angle models or different sizes, are depicted with reference to the initial radii of the droplets. Between the quasi-static and the Kistler mode, the latter is showing more pronounced decrease in the jumping velocity. However, the comparison of both models to the no-hysteresis gives a more profound difference. Lastly, to the Kistler model behavior, it is needed to mention that the moments of receding behavior showed the lowest contact angles and the most dissipation of energy in the system. Therefore, it is concluded that a comprehensive study which has validated its hysteresis connection to experimental data, showed increased dissipation due to hysteresis.

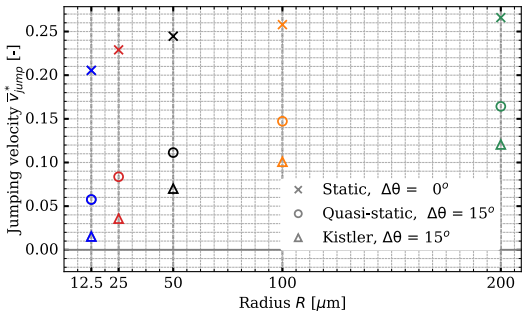

Figure 4.4: Jumping velocities v^*_{jump} at different radius. The jumping velocity as a function of initial droplet radius with three contact-angle implementations, without hysteresis, with static hysteresis (Quasi-static) and dynamic contact model (Kistler). For a surface that showshysteresis, an equilibrium static contact angle can overpredict the jumping velocity.

The study, in addition, agreed with former experimental studies, that targeted a minimum hysteresis with the manufacturing of new superhydrophobic surfaces in order to achieve maximum energy conversion in the jumping process.

4.3 Paper C

In paper C, the study investigates the particle-droplet mechanism. We introduced a steel particle, following a case in the experimental publication[25], with size $R_p = 80$ µand a droplet with initial radius $R_d = 120$ µm. The details on the numerical setup have been provided in Chapter 3 and the configuration is available on the corresponding section in Paper B. We aim to understand how the released surface energy and the acting forces interact during the process where a single droplet merges with a particle. In Figure 4.5 a comparison of experimental and numerical images at the same instant is made. They show that the model accurately replicates critical stages of the particle-droplet interaction, including coalescence, capillary wave motion, and the final jumping phase. This side-by-side validation underscores the model's capability in simulating complex droplet oscillations and particle motion, con-

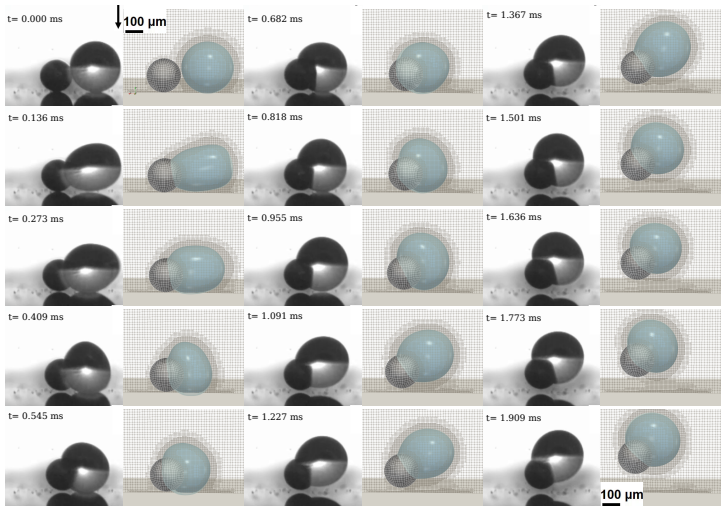

Figure 4.5: Comparison of numerical simulation with particle jumping against experimental images by Yan et al.[25]. The particle has radius $R_p = 80$ µm and the droplet $R_d = 120$ µm. The positions of the objects in the numerical instants match the ones in the experiment. The top left image denotes gravity direction. Reprinted (adapted) with permission from ACS Nano 16, 8 (2022). Copyright 2022 American Chemical Society.

firming the framework's ability in capturing the particle adhesion and jumping with the droplet.

The velocity of the system is studied, formulated as kinetic energy. We distinguish the kinetic energy as computed from the upwards vertical velocity of the system, the kinetic energy of the droplet and the particle from their individual translational velocity magnitudes and the oscillation kinetic energy of the droplet, which is the total droplet energy subtracting the translational droplet energy. In Figure 3 of Paper B each mode is provided, within the grid validation study that was performed for the article. The study tested three levels of grid refinement (20, 30, and 40 cells per droplet diameter) and demonstrated consistent energy behavior for the finer grids, validating that the chosen resolution (30 cells per droplet diameter) captures the energy dynamics efficiently without unnecessary computational demand. This finding supports using this grid size in further simulations to balance accuracy and efficiency.

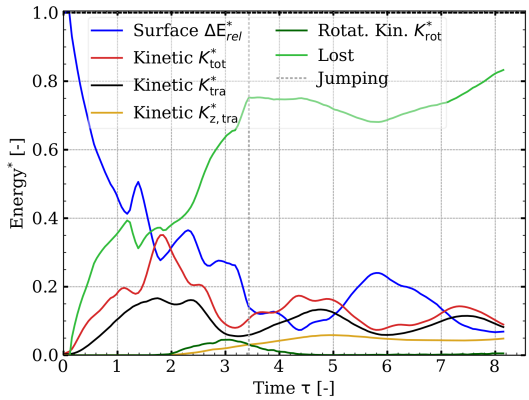

Figure 4.6: Energy budget obtained by the simulation of particle-droplet jumping from Figure 4.5. The released surface energy ΔE^*_{rel} is presented normalized by the total available energy in the system. In addition, it is offered the translational kinetic energy of the particle and the droplet K^*_{tra} and the total kinetic energy of the system K^*_{tot}. The upwards kinetic energy of the system (in z direction) is presented as $K^*_{\mathrm{z,\,tra}}$ with orange and the rotational kinetic energy of the system K^*_{rot} is also available. Finally, the losses in the system are plotted as measured by subtracting the available surface energy and the kinetic energies from the total available energy of the system. The vertical dotted gray line is the instant of detachment.

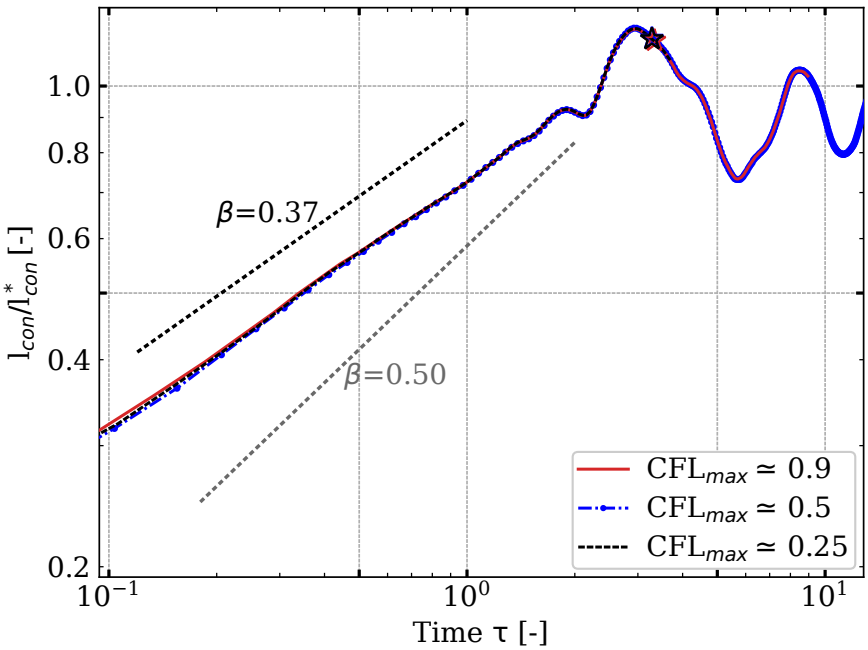

Figure 4.7: Normalized arch lengths of spreading over time. Three different time-steps are evaluated showcasing time-step convergence. The spreading has a constant exponential rate with the spreading factor of $\beta = 0.37$. The asterisk shows the jump of the particle-droplet system.

The energy amounts in the system have been compared with an approach that pinpoints the surface energy at any time of the simulation and subtracts it from the initial surface energy. In Figure 4.6 the energy balance for the case of the video images is presented. The total kinetic energy is superimposed to understand what was the maximum energy passed to the droplet and the particle at any point of the simulation. After detachment the kinetic energy in the system reduces due to viscous dissipation and due to the damping of the oscillations for the droplet.

Regarding the particle-droplet jumping mechanism, a study was also performed in the initial spreading of the droplet across the spherical surface of the particle. Details on how the spreading area was computed are offered

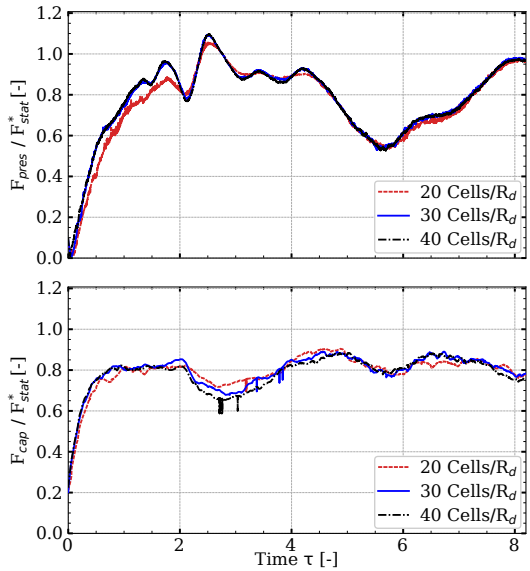

Figure 4.8: Computed hydrodynamic forces due to pressure and capillary adhesive forces obtained from the simulation (magnitude) for three different grid resolutions. The forces are normalized by the ideal capillary force at rest.

in Paper C. Figure 4.7 shows the droplet's normalized spreading length on a particle surface, from the arch length of the contact area. During spreading stage, the length l_{con} is increasing with an exponential rate, with near constant factor $\beta \simeq 0.37$. This value is compared to the experiment of Yan et al. which computed it to be between $\beta \simeq 0.4 - 0.7$ when different particle-droplet pairs were tested. Moreover, it is within the range $0.25 - 0.66$m that other numerical studies suggested for spreading on curved surfaces or planes. In the figure present, a comparison of three different time-steps was available, to emphasize that the simulations show convergence for the time-step that was selected within the rest studies. The spreading was the most dynamical process of the system, and offers a strong example of the time-step influence in the whole particle-droplet jumping mechanism.

Figure 4.8 depicts the hydrodynamic and capillary forces against simulation time, that are enforced on the particle during the wetting from the droplet.

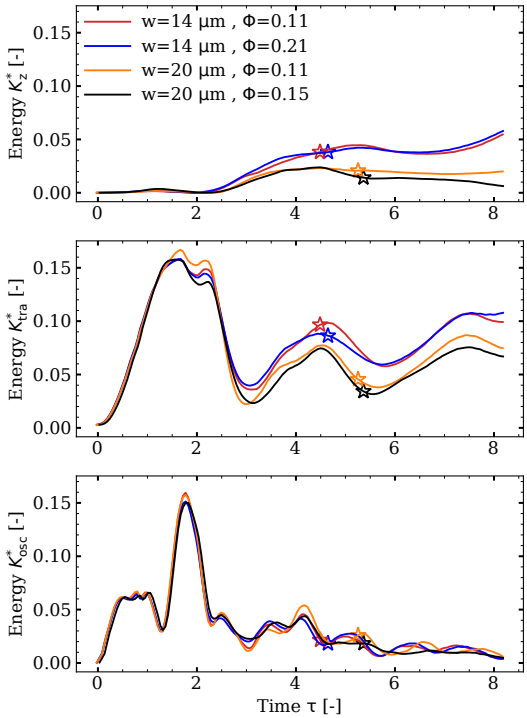

Figure 4.9: Top to bottom sequence: Upwards (z-direction) kinetic energy, translational kinetic energy of particle and droplet, and oscillational kinetic energy of droplet in the mechanism of particle-droplet jumping for 4 different pillars configurations of width (w) and solid area ratio (Φ). The plots suggest that energy is dissipated in the cases of wider pillars, while the pitch between pillars has a reduced influence. The asterisk symbols indicate the moment of jumping.

The forces were compared across three grid sizes, a case with 20 cells per radius at maximum refinement, with 30 and 40 cells. It is noticed the oscillatory pattern of the forces following the increase during initial spreading. The capillary force is responsible for capturing the particle and is modeled with the adopted CCF method, presented in Chapter 3. Its magnitude is within the same mean value as the hydrodynamic force, while the contact line oscillates around the location of the ideal wetting area. In the figure the forces were

normalized by the ideal capillary force at rest, and the finer grids (30 and 40 cells per droplet radius) yielded very close force magnitudes. The results emphasize the role of capillary forces in achieving successful detachment, as larger forces facilitate the particle-droplet launch from the substrate.

4.4 Paper D

In the last study of the project, rectangular pillars were introduced on top of the superhydrophobic surface, with equally spacing between the pillars. The complexity for the numerical framework was therefore increased and the pillars were modeled with the IBM. The intrinsic wettability of such structures that offer superhydrophobicity is hydrophobic, and an analogous contact angle ($\theta_{eq} = 105°$) was imposed. The mechanism of particle-droplet jumping was then introduced for first time into such a surface, whereas similar studies has been performed for the binary droplet jumping case. As the droplet, in a case with same particle and droplet properties as in Paper C, spreads on the particle, it then interacts with the hydrophobic surfaces of the pillars, expanding and wetting the top of the pillars, before jumping. With this research, it was targeted to examine how the different superhydrophobic surfaces with micro-structures of various dimensions and spacing, change the outcome on the particle jumping.

In the first part of the study it was highlighted the ability to showcase jumping for the particle-droplet system, in a surface configuration that follows the literature for suitable width, stepping and solid area fraction. The result was compared with the case from Paper C for its velocity variation and for a comparison of video images from the simulation, which further included the experimental images too. The jumping occurred at slightly later instant with reduced velocity. Following this validation on jumping possibility (further details in Paper D), we compared the velocities behavior for the particle-droplet system, where the superhydrophobic surface would adopt 4 different configurations. The kinetic energies are available in Figure 4.9 and suggested that for wider pillars the particle jumped with reduced velocity. In Paper D, the evolution of the contact area, length of contact line and mean contact angle are additionally offered. The increased energy dissipation was connected with the larger contact area between droplet and superhydrophobic surface both on top, but also noted at the pillar's side areas. By contrast, altering

the pitch size (the stepping between pillars) had a less pronounced effect, with larger spacing only showing marginal increases in jumping efficiency. Therefore, it is suggested that the characteristic width of pillars, relative to the size of the droplets for each application is of higher importance and it should be optimized in the manufacturing of functioning micro-structured superhydrophobic surfaces.

Moreover, a study on height of the pillars was undertaken and we consider important to emphasize it in the selected results since such a variation in the surface produced a considerable influence on the jumping outcome. A list of selected instants in a close-up view is available in Figure 4.10. The longer void between the liquid meniscus of the interface, formed between two pillars, and the bottom of the surface promoted a faster retraction and led to higher jumping velocity. A similar study was performed for the intrinsic wettability of the pillars. The contact angle was reduced from $\theta_{eq} = 105^\circ$ to $\theta_{eq} = 90^\circ$ and a comparison of the two cases focused in the evolution of the kinetic energies and the overall behavior of the system with three-dimensional images. The comparison (available in Figure 4.11) showed that, at lower contact angle, the droplet loses its ability to stay suspended on the pillars throughout the processes of spreading and capturing the particle, leading to a transition to Wenzel wetting state from initial Cassie-Baxter. The resulted enhanced dissipation due to wetting the surface prevented the detachment of the particle-droplet system. As a conclusive remark from this study, superhdyrophobic surfaces that would enhance self-cleaning with droplets, would require sufficiently tall and narrow pillars with adequate hydrophobicity at their nanoscale.

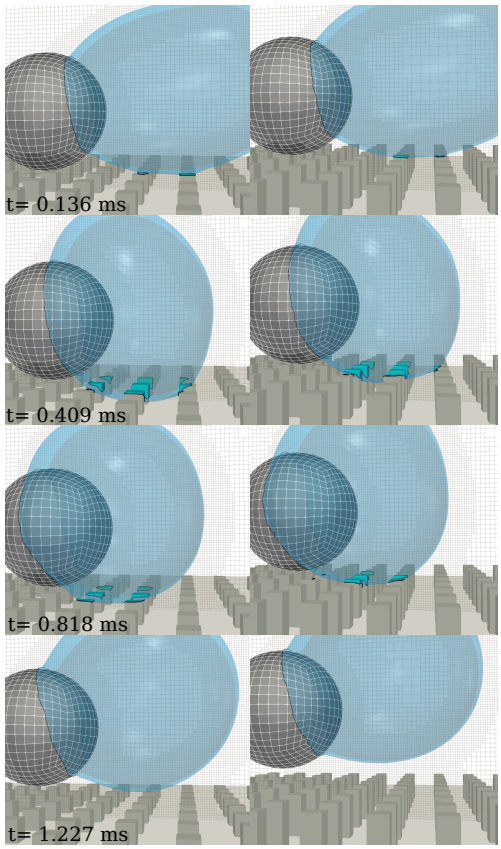

Figure 4.10: Video instants of the droplet spreading on the particle and the particle-droplet jumping for substrates with pillar heights $h = 24$ µm (left images)and 45 µm (right images) — with $R_p = 80$ µm and $R_d = 120$ µm. The contact area with the pillars is highlighted and the contact line is visualized with black curve. The droplet reaches closer to the bottom of the substrate for the case with the shorter pillars and the particle-droplet system obtained a reduced jumping velocity.

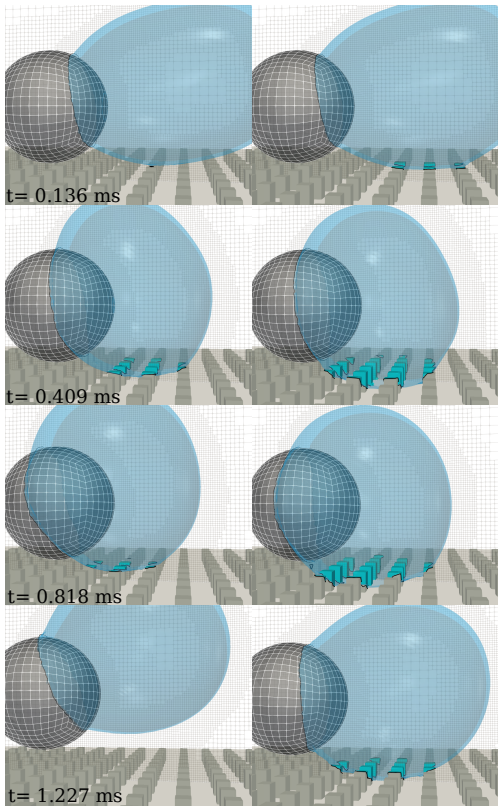

Figure 4.11: Video instants of the droplet spreading on the particle and the particle-droplet jumping for substrates with implented contact angles $\theta_{eq} = 105°$ (left images and 90° µm (right images) — with $R_p = 80$ µm and $R_d = 120$ µm. The contact area with the pillars is highlighted and the contact line is visualized with black curve. The case with the lower contact angle fully wetted the substrate, whereas the system adhered to the structured surface.

CHAPTER 5

Conclusions and future work

5.1 Conclusions

This thesis explores fundamental physical processes and mechanisms responsible for self-cleaning of superhydrophobic surfaces. Two mechanisms were the focus of the thesis; i) a jumping droplet upon coalescence of two or more droplets and ii) a particle-droplet jumping, which occurs following a spontaneous spreading of a droplet on a solid particle resting on a superhydrophobic surface. By applying numerical simulations and formulating a series of case studies, a comprehensive framework has been developed and validated, progress has been achieved in understanding the adhesion of particles on droplets and, finally, guidelines have been provided regarding the needed wetting properties of superhydrophobic surfaces, including the optimum designs of surfaces with deposited micro-structures. This section reviews the main findings of each study and how they contributed to the objectives of this work.

Paper A starts with a literature review on the phenomenon of coalescence and jumping of droplets from superhydrophobic surfaces, highlighting the jumping velocities and the cut-off radius below which droplets do not

jump, and comparing the findings of other works for the case of microdroplets ($R < 25$ μm). Following a validation of the VOF-based numerical framework using experimental data and previous numerical works, simulations at different length scales were performed to explain the influence of simplified wetting models on the jumping efficiency, as well as to compare the interchange of surface tension, inertia and viscous effects. They key finding was that microdroplets as small as 0.5 μm were able to jump, amid with a reduced efficiency, and, as a result, that the primary cause for the existence of a cut-off radius is not the viscous forces but the interaction with the micro-scale geometrical features of the superhydrophobic surfaces. These findings support our objective to provide quantitative insights into the dynamics of both the coalescence and jumping parts of the entire mechanism.

Paper B focuses on the effect of the contact-angle hysteresis and how effectively the jumping of coalescing droplets can be captured within the framework, which uses modeling to predict the contact angle and the dynamics of the moving contact line. Following validation studies that focused both on the detailed capturing of dynamics of a sharp interface and on jumping from superhydrophobic surfaces with a recorded hysteresis – by comparing to corresponding experimental studies – it was found that hysteresis impacts the jumping droplets process by delaying detachment, followed by a re-attachment event on the surface, before eventual jumping with a significantly reduced upwards kinetic energy. Additionally, the jumping process has been studied at different spatial scales in order to observe at which droplet radius the process exhibits a stronger dissipation stemming from the contact angles. Implementation of a dynamic contact model enhances hysteresis, reducing the values applied at the receding phase of the merged droplet from the surface and minimizing the jumping ability. In general, the results showcase a strong sensitivity of the jumping velocity on the values of the implemented contact angles. By analyzing the restrictive nature of contact-angle hysteresis, this paper provides critical insights into the need for the existence of low-hysteresis surfaces in applications requiring a rapid droplet removal.

Paper C examines the mechanism of particle-droplet coalescence and jumping, becoming the first numerical study that succeeded in capturing the spreading of a droplet onto a solid particle, its interaction with the superhydrophobic surface and the eventual jumping of a particle-droplet system. A coupled VOF-IBM framework was enhanced with a rigid-body dynamic solver for the

computation of forces on the particle surface and with a suggested representation of a capillary force, an extension of the Capillary Continuum Force method by Washino et al.[97]. This representation has been validated with great agreement against experimental images of the process provided by Yan et al.[25]. The subsequent case studies varied the physical properties of the droplet, the particle and the wettability of both the superhydrophobic surface and the solid particle. The study has been able to identify the effect of contact angles, suggesting that superhydrophobicity with a low degree of hysteresis plays an important role in the jumping velocity. Similarly, the hydrophilic nature of the contaminant particle enhanced the jumping efficiency. Moreover, the energy budget has been studied in order to observe the rate of release of the available surface energy in the system in relation to the kinetic energy absorbed. Finally, there were studies regarding the influence of a range of properties, such as the viscosity and the particle density, the particle-droplet size ratio. An increased rate of dissipation was identified when the droplet was significantly larger than the particle or when it was smaller or of a similar size to a significantly heavier particle. This study thus validated the introduced numerical models for complex droplet-particle interactions, confirming the robustness of the framework, and provided guidelines for the design of functional surfaces for various technological applications.

Paper D concludes the work in this thesis and evaluates for the mechanism of particle-droplet coalescence and jumping the influence of micro-pillars that are present on structured superhydrophobic surfaces. Following a grid independence study, the simulations affirmed the superhydrophobic behavior of such surfaces. The particle-droplet system was able to jump, following the same stages of the process as the ones appearing for smoothed surfaces, modeled with extreme superhydrophobic contact angles. Then, a series of surfaces with differing pillar configurations were studied, with the results suggesting that the width of the pillars significantly affects the energy dissipation. Similarly, the jumping was more efficient when using higher pillars that hindered the wetting of the bottom of the surface. When significantly reducing the contact angle of the pillars, it has been shown a transition from a Cassie-Baxter to a Wenzel wetting state that fully wetted the bottom of the surface and adhered the particle-droplet system to the surface. In the latter case, the particle-droplet system did not jump. Therefore, this research provided knowledge on the wetting dynamics of structured superhydrophobic surfaces

and was able to characterize the dimensions for the micro-pillars that enable the design of surfaces with enhanced self-cleaning properties.

To summarize, the thesis successfully achieved its objectives, advancing the understanding of self-cleaning mechanisms on superhydrophobic surfaces through comprehensive simulation studies. The presented results not only validated the proposed numerical models but also offered practical guidelines for designing surfaces that facilitate self-cleaning properties. Each study demonstrated the important role that factors such as the droplet size, contact-angle hysteresis, particle properties and interactions, and surface microstructures play in either facilitating or limiting droplet detachment and contaminant removal. The validated framework proved effective for capturing intricate interactions present in droplet-particle-superhydrophobic surface systems. The studies yielded quantitative insights into optimizing surface properties, including designing low-hysteresis surfaces for a rapid droplet removal, using specific microstructure configurations to enhance the jumping efficiency, and tailoring particle-droplet size ratios to reduce energy losses. This work provides the base for advancing superhydrophobic surface designs tailored to various industrial applications and demonstrates the benefits of using advanced numerical modeling for developing high-performance, self-cleaning surfaces.

5.2 Future work

With the completion of this study, progress has been made regarding our understanding of the fundamentals of the interaction of micrometer- sized droplets with superhydrophobic surfaces and spherical solid particles. In addition, detailed information is provided on the topic of evolution of coalescence of two or more droplets and the coalescence-induced oscillations of the merged droplet. Finally, valuable knowledge is gained regarding the behavior of an oscillating droplet interacting with pillared structures that cause superhydrophobicity under certain conditions. Future studies will have the ability to build on the work presented in this thesis by implementing and validating various adhesion properties for a list of extended configurations such as generic-shaped solid particles, different pillar shapes and their placement strategies, introduction of multiple droplets and particles, as well as actual solid substrates with geometries provided by three-dimensional laser scanning.

In the final phase of this work, an intriguing idea on understanding and characterizing elasticity deformations of pillars or other surface singularity points has been proposed. The idea behind this study would be to obtain more knowledge for the behavior of the contact line and of the capillary stresses acting at it, when the pillars undergo deformation. It would be of great interest to find out whether the contact line shows more frequent pinning occurrences or whether droplet and particle jumping mechanisms dissipate more energy due to such solid motion. Moreover, information could be provided on the behavior of capillary forces on hydrophilic surfaces, such as the solid particle, answering the potential of peak forces in the case of elastic deformation or other types of existing surface singularities. The framework developed in this study, which utilizes the immersed boundary method and the coupling with solid mechanics and a rigid-body motion solver, is considered vital to perform such analyses. Finally, even though numerical simulations themselves provide important information, future studies could be useful for developing new experimental tools, that would allow the measurement of loads on points of structured surfaces and locate and track the contact line at time-scales that the current experimental configurations do not capture. This will help in validating the simulations at length-scales smaller than the ones presented in the current thesis, where the continuum approach starts to approach its definition limit.

References

[1] D. Quéré, "Non-sticking drops," *Reports on Progress in Physics*, vol. 68, no. 11, pp. 2495–2532, Sep. 2005, ISSN: 00344885.

[2] C. Antonini, A. Amirfazli, and M. Marengo, "Drop impact and wettability: From hydrophilic to superhydrophobic surfaces," *Physics of Fluids*, vol. 24, no. 10, 2012, ISSN: 10706631.

[3] P. Roach, N. J. Shirtcliffe, and M. I. Newton, "Progess in superhydrophobic surface development," *Soft Matter*, vol. 4, no. 2, p. 224, Jan. 2008, ISSN: 17446848.

[4] N. Miljkovic, R. Enright, Y. Nam, *et al.*, "Jumping-droplet-enhanced condensation on scalable superhydrophobic nanostructured surfaces," *Nano Letters*, vol. 13, no. 1, pp. 179–187, Jan. 2013, ISSN: 15306984.

[5] N. Miljkovic, R. Enright, and E. N. Wang, "Modeling and Optimization of Superhydrophobic Condensation," *Journal of Heat Transfer*, vol. 135, no. 11, pp. 111004–1 – 111004–14, Nov. 2013, ISSN: 0022-1481.

[6] K. M. Wisdom, J. A. Watson, X. Qu, F. Liu, G. S. Watson, and C.-H. Chen, "Self-cleaning of superhydrophobic surfaces by self-propelled jumping condensate," *Proceedings of the National Academy of Sciences*, vol. 110, no. 20, pp. 7992–7997, May 2013, ISSN: 0027-8424.

[7] Q. Wang, X. Yao, H. Liu, D. Quéré, and L. Jiang, "Self-removal of condensed water on the legs of water striders," *Proceedings of the National Academy of Sciences of the United States of America*, vol. 112, no. 30, pp. 9247–9252, 2015, ISSN: 10916490.

[8] D. Maggiolo, M. Seemann, H. Thunman, *et al.*, "Self-Cleaning Surfaces for Heat Recovery During Industrial Hydrocarbon-Rich Gas Cooling: An Experimental and Numerical Study," *AIChE Journal*, vol. 65, no. 1, pp. 317–325, Jan. 2019, ISSN: 15475905.

[9] S. P. Dalawai, M. A. Saad Aly, S. S. Latthe, *et al.*, "Recent Advances in durability of superhydrophobic self-cleaning technology: A critical review," *Progress in Organic Coatings*, vol. 138, p. 105 381, Jan. 2020, ISSN: 0300-9440.

[10] C. Yu, S. Sasic, K. Liu, S. Salameh, R. H. Ras, and J. R. van Ommen, "Nature–Inspired self–cleaning surfaces: Mechanisms, modelling, and manufacturing," *Chemical Engineering Research and Design*, vol. 155, pp. 48–65, Mar. 2020, ISSN: 02638762.

[11] H. Wang, L. Tang, X. Wu, W. Dai, and Y. Qiu, "Fabrication and anti-frosting performance of super hydrophobic coating based on modified nano-sized calcium carbonate and ordinary polyacrylate," *Applied Surface Science*, vol. 253, no. 22, pp. 8818–8824, Sep. 2007, ISSN: 01694332.

[12] S. Farhadi, M. Farzaneh, and S. A. Kulinich, "Anti-icing performance of superhydrophobic surfaces," *Applied Surface Science*, vol. 257, no. 14, pp. 6264–6269, May 2011, ISSN: 01694332.

[13] S. A. Kulinich and M. Farzaneh, "Effect of contact angle hysteresis on water droplet evaporation from super-hydrophobic surfaces," *Applied Surface Science*, vol. 255, no. 7, pp. 4056–4060, 2009, ISSN: 01694332.

[14] D. Bonn, J. Eggers, J. Indekeu, and J. Meunier, "Wetting and spreading," *Reviews of Modern Physics*, vol. 81, no. 2, pp. 739–805, 2009, ISSN: 15390756.

[15] S. Popinet, "Numerical Models of Surface Tension," *Annual Review of Fluid Mechanics*, vol. 50, no. 1, pp. 49–75, 2018, ISSN: 0066-4189.

[16] P.-G. de Gennes, F. Brochard-Wyart, and D. Quéré, *Capillarity and Wetting Phenomena*. Springer New York, 2004, ISBN: 9781441918338.

[17] S. Nishimoto and B. Bhushan, "Bioinspired self-cleaning surfaces with superhydrophobicity, superoleophobicity, and superhydrophilicity," *RSC Advances*, vol. 3, no. 3, pp. 671–690, 2013, ISSN: 20462069.

[18] D. Öner and T. J. McCarthy, "Ultrahydrophobic surfaces. Effects of topography length scales on wettability," *Langmuir*, vol. 16, no. 20, pp. 7777–7782, Oct. 2000, ISSN: 07437463.

[19] J. Wu, J. Xia, W. Lei, and B.-p. Wang, "Advanced understanding of stickiness on superhydrophobic surfaces," *Scientific Reports*, vol. 3, no. 1, p. 3268, Dec. 2013, ISSN: 2045-2322.

[20] Y. Liu and C. H. Choi, "Condensation-induced wetting state and contact angle hysteresis on superhydrophobic lotus leaves," *Colloid and Polymer Science*, vol. 291, no. 2, pp. 437–445, Feb. 2013, ISSN: 0303402X.

[21] J. E. Sprittles and Y. D. Shikhmurzaev, "Coalescence of liquid drops: Different models versus experiment," *Physics of Fluids*, vol. 24, no. 12, p. 122 105, Dec. 2012, ISSN: 1070-6631.

[22] D. Quéré, "Wetting and roughness," *Annual Review of Materials Research*, vol. 38, pp. 71–99, 2008, ISSN: 15317331.

[23] C. W. Lo, Y. C. Chu, M. H. Yen, and M. C. Lu, "Enhancing Condensation Heat Transfer on Three-Dimensional Hybrid Surfaces," *Joule*, vol. 3, no. 11, pp. 2806–2823, 2019, ISSN: 25424351.

[24] N. Miljkovic, R. Enright, and E. N. Wang, "Effect of droplet morphology on growth dynamics and heat transfer during condensation on superhydrophobic nanostructured surfaces," *ACS Nano*, vol. 6, no. 2, pp. 1776–1785, 2012, ISSN: 19360851.

[25] X. Yan, B. Ji, L. Feng, *et al.*, "Particulate-Droplet Coalescence and Self-Transport on Superhydrophobic Surfaces," *ACS Nano*, vol. 16, no. 8, pp. 12 910–12 921, Aug. 2022, ISSN: 1936086X.

[26] W. Barthlott and C. Neinhuis, "Purity of the sacred lotus, or escape from contamination in biological surfaces," *Planta*, vol. 202, no. 1, pp. 1–8, 1997, ISSN: 1432-2048.

[27] C. W. Extrand and S. I. Moon, "Repellency of the lotus leaf: Contact angles, drop retention, and sliding angles," *Langmuir*, vol. 30, no. 29, pp. 8791–8797, Jul. 2014, ISSN: 15205827.

[28] D. Khojasteh, M. Kazerooni, S. Salarian, and R. Kamali, "Droplet impact on superhydrophobic surfaces: A review of recent developments," *Journal of Industrial and Engineering Chemistry*, vol. 42, pp. 1–14, 2016, ISSN: 22345957.

[29] X. Yan, Z. Huang, S. Sett, *et al.*, "Atmosphere-Mediated Superhydrophobicity of Rationally Designed Micro/Nanostructured Surfaces," *ACS Nano*, vol. 13, no. 4, pp. 4160–4173, Apr. 2019, ISSN: 1936-0851.

[30] E. B. Dussan, "On the Spreading of Liquids on Solid Surfaces: Static and Dynamic Contact Lines," *Annual Review of Fluid Mechanics*, vol. 11, no. 1, pp. 371–400, Jan. 1979, ISSN: 0066-4189.

[31] J. H. Snoeijer and B. Andreotti, "Moving Contact Lines: Scales, Regimes, and Dynamical Transitions," *Annual Review of Fluid Mechanics*, vol. 45, no. 1, pp. 269–292, 2013, ISSN: 0066-4189.

[32] W. Ren and W. E, "Boundary conditions for the moving contact line problem," *Physics of Fluids*, vol. 19, no. 2, p. 022 101, Feb. 2007, ISSN: 1070-6631.

[33] B. Bhushan and Y. C. Jung, "Wetting, adhesion and friction of superhydrophobic and hydrophilic leaves and fabricated micro/nanopatterned surfaces," *Journal of Physics Condensed Matter*, vol. 20, no. 22, p. 225 010, Apr. 2008, ISSN: 09538984.

[34] R. Enright, N. Miljkovic, J. L. Alvarado, K. Kim, and J. W. Rose, "Dropwise condensation on micro-and nanostructured surfaces," *Nanoscale and Microscale Thermophysical Engineering*, vol. 18, no. 3, pp. 223–250, 2014, ISSN: 15567265.

[35] D. Wang, Q. Sun, M. J. Hokkanen, *et al.*, "Design of robust superhydrophobic surfaces," *Nature*, vol. 582, no. 7810, pp. 55–59, 2020, ISSN: 14764687.

[36] T. Mouterde, G. Lehoucq, S. Xavier, *et al.*, "Antifogging abilities of model nanotextures," *Nature Materials*, vol. 16, no. 6, pp. 658–663, Jun. 2017, ISSN: 1476-1122.

[37] Y. C. Jung and B. Bhushan, "Dynamic Effects of Bouncing Water Droplets on Superhydrophobic Surfaces," *Langmuir*, vol. 24, no. 12, pp. 6262–6269, Jun. 2008, ISSN: 0743-7463.

[38] Y. Sun, Y. Jiang, C.-H. Choi, G. Xie, Q. Liu, and J. W. Drelich, "Direct Measurements of Adhesion Forces for Water Droplets in Contact with Smooth and Patterned Polymers," *Surface Innovations*, vol. 6, no. 1-2, pp. 1–52, Oct. 2017, ISSN: 2050-6252.

[39] A. B. D. Cassie and S. Baxter, "Wettability of porous surfaces," *Transactions of the Faraday society*, vol. 40, pp. 546–551, 1944.

[40] Q. Hao, Y. Pang, Y. Zhao, J. Zhang, J. Feng, and S. Yao, "Mechanism of Delayed Frost Growth on Superhydrophobic Surfaces with Jumping Condensates: More Than Interdrop Freezing," *Langmuir*, vol. 30, no. 51, pp. 15 416–15 422, Dec. 2014, ISSN: 0743-7463.

[41] X. Yan, F. Chen, S. Sett, *et al.*, "Hierarchical Condensation," *ACS Nano*, vol. 13, no. 7, pp. 8169–8184, Jul. 2019, ISSN: 1936086X.

[42] C. Lv, P. Hao, X. Zhang, and F. He, "Dewetting Transitions of Dropwise Condensation on Nanotexture-Enhanced Superhydrophobic Surfaces," *ACS Nano*, vol. 9, no. 12, pp. 12 311–12 319, 2015, ISSN: 1936086X.

[43] R. Mukherjee, A. S. Berrier, K. R. Murphy, J. R. Vieitez, and J. B. Boreyko, "How Surface Orientation Affects Jumping-Droplet Condensation," *Joule*, vol. 3, no. 5, pp. 1360–1376, 2019, ISSN: 25424351.

[44] D. J. Preston, D. L. Mafra, N. Miljkovic, J. Kong, and E. N. Wang, "Scalable graphene coatings for enhanced condensation heat transfer," *Nano Letters*, vol. 15, no. 5, pp. 2902–2909, May 2015, ISSN: 15306992.

[45] X. Yan, L. Zhang, S. Sett, *et al.*, "Droplet Jumping: Effects of Droplet Size, Surface Structure, Pinning, and Liquid Properties," *ACS Nano*, vol. 13, no. 2, pp. 1309–1323, Feb. 2019, ISSN: 1936086X.

[46] L. Xia, H. Yu, F. Chen, Z. Huo, D. Zhang, and Y. Tian, "Pillar height regulated droplet impact dynamics on pillared superhydrophobic surfaces," *International Journal of Mechanical Sciences*, vol. 276, p. 109 386, Aug. 2024, ISSN: 0020-7403.

[47] P. G. De Gennes, "Wetting: statics and dynamics," *Reviews of Modern Physics*, vol. 57, no. 3, pp. 827–863, Jul. 1985, ISSN: 00346861.

[48] D. Legendre and M. Maglio, "Computers & Fluids Comparison between numerical models for the simulation of moving contact lines," *Computers and Fluids*, vol. 113, pp. 2–13, 2015, ISSN: 0045-7930.

[49] R. Enright, N. Miljkovic, N. Dou, Y. Nam, and E. N. Wang, "Condensation on Superhydrophobic Copper Oxide Nanostructures," *Journal of Heat Transfer*, vol. 135, no. 9, Sep. 2013, ISSN: 0022-1481.

[50] F. Chu, X. Yan, and N. Miljkovic, "How Superhydrophobic Grooves Drive Single-Droplet Jumping," *Langmuir*, vol. 38, no. 14, pp. 4452–4460, Apr. 2022, ISSN: 15205827.

[51] H. Cha, C. Xu, J. Sotelo, *et al.*, "Coalescence-induced nanodroplet jumping," *Physical Review Fluids*, vol. 1, no. 6, p. 064 102, Oct. 2016, ISSN: 2469-990X.

[52] M. D. Mulroe, B. R. Srijanto, S. F. Ahmadi, C. P. Collier, and J. B. Boreyko, "Tuning Superhydrophobic Nanostructures To Enhance Jumping-Droplet Condensation," *ACS Nano*, vol. 11, no. 8, pp. 8499–8510, Aug. 2017, ISSN: 1936-0851.

[53] L. B. Boinovich and A. M. Emelyanenko, "Anti-icing potential of superhydrophobic coatings," *Mendeleev Communications*, vol. 23, no. 1, pp. 3–10, Jan. 2013, ISSN: 09599436.

[54] H. Cha, S. Sett, P. Birbarah, T. Gebrael, J. Oh, and N. Miljkovic, *Recent advances in structured surface enhanced condensation heat transfer*. IOP Publishing, Mar. 2020, pp. 13–1–13–32, ISBN: 9780750317382.

[55] N. Miljkovic, D. J. Preston, R. Enright, and E. N. Wang, "Jumping-droplet electrostatic energy harvesting," *Applied Physics Letters*, vol. 105, no. 1, Jul. 2014, ISSN: 0003-6951.

[56] K. A. Raman, E. Birgersson, Y. Sui, and A. Fisher, "Electrically induced droplet ejection dynamics under shear flow," *Physics of Fluids*, vol. 32, no. 3, p. 032 103, Mar. 2020, ISSN: 10897666.

[57] X. Gao, X. Yao, and L. Jiang, "Effects of rugged nanoprotrusions on the surface hydrophobicity and water adhesion of anisotropic micropatterns," *Langmuir*, vol. 23, no. 9, pp. 4886–4891, 2007, ISSN: 07437463.

[58] Q. Peng, L. Jia, Y. Ding, C. Dang, L. Yin, and X. Yan, "Influence of groove orientation on dropwise condensation on hydrophobic and hierarchical superhydrophobic surfaces with microgroove arrays," *International Communications in Heat and Mass Transfer*, vol. 112, no. January, p. 104 492, 2020, ISSN: 07351933.

[59] S. Moghtadernejad, M. Tembely, M. Jadidi, N. Esmail, and A. Dolatabadi, "Shear driven droplet shedding and coalescence on a superhydrophobic surface," *Physics of Fluids*, vol. 27, no. 3, 2015, ISSN: 10897666.

[60] J. B. Boreyko and C. H. Chen, "Self-propelled dropwise condensate on superhydrophobic surfaces," *Physical Review Letters*, vol. 103, no. 18, pp. 2–5, 2009, ISSN: 00319007.

[61] F. Liu, G. Ghigliotti, J. J. Feng, and C.-H. Chen, "Numerical simulations of self-propelled jumping upon drop coalescence on non-wetting surfaces," *Journal of Fluid Mechanics*, vol. 752, pp. 39–65, Aug. 2014, ISSN: 0022-1120.

[62] K. Rykaczewski, A. T. Paxson, S. Anand, X. Chen, Z. Wang, and K. K. Varanasi, "Multimode multidrop serial coalescence effects during condensation on hierarchical superhydrophobic surfaces," *Langmuir*, vol. 29, no. 3, pp. 881–891, 2013, ISSN: 07437463.

[63] Y. Nam, H. Kim, and S. Shin, "Energy and hydrodynamic analyses of coalescence-induced jumping droplets," *Applied Physics Letters*, vol. 103, no. 16, p. 161 601, Oct. 2013, ISSN: 0003-6951.

[64] F. Liu, G. Ghigliotti, J. J. Feng, and C. H. Chen, "Self-propelled jumping upon drop coalescence on leidenfrost surfaces," *Journal of Fluid Mechanics*, vol. 752, pp. 22–38, 2014, ISSN: 14697645.

[65] K. Yanagisawa, M. Sakai, T. Isobe, S. Matsushita, and A. Nakajima, "Investigation of droplet jumping on superhydrophobic coatings during dew condensation by the observation from two directions," *Applied Surface Science*, vol. 315, no. 1, pp. 212–221, 2014, ISSN: 01694332.

[66] R. Attarzadeh and A. Dolatabadi, "Coalescence-induced jumping of micro-droplets on heterogeneous superhydrophobic surfaces," *Physics of Fluids*, vol. 29, no. 1, p. 012 104, Jan. 2017, ISSN: 1070-6631.

[67] J. Wasserfall, P. Figueiredo, R. Kneer, W. Rohlfs, and P. Pischke, "Coalescence-induced droplet jumping on superhydrophobic surfaces: Effects of droplet mismatch," *Physical Review Fluids*, vol. 2, no. 12, p. 123 601, Dec. 2017, ISSN: 2469-990X.

[68] F. Chu, Z. Yuan, X. Zhang, and X. Wu, "Energy analysis of droplet jumping induced by multi-droplet coalescence: The influences of droplet number and droplet location," *International Journal of Heat and Mass Transfer*, vol. 121, pp. 315–320, 2018, ISSN: 00179310.

[69] H. Vahabi, W. Wang, J. M. Mabry, and A. K. Kota, "Coalescence-induced jumping of droplets on superomniphobic surfaces with macrotexture," *Science Advances*, vol. 4, no. 11, eaau3488, Nov. 2018, ISSN: 2375-2548.

[70] Z. Yuan, R. Wu, and X. Wu, "Numerical simulations of multi-hop jumping on superhydrophobic surfaces," *International Journal of Heat and Mass Transfer*, vol. 135, pp. 345–353, 2019, ISSN: 00179310.

[71] Y. Wang and P. Ming, "Dynamic and energy analysis of coalescence-induced self-propelled jumping of binary unequal-sized droplets," *Physics of Fluids*, vol. 31, no. 12, p. 122 108, Dec. 2019, ISSN: 1070-6631.

[72] S. Li, F. Chu, J. Zhang, D. Brutin, and D. Wen, "Droplet jumping induced by coalescence of a moving droplet and a static one: Effect of initial velocity," *Chemical Engineering Science*, vol. 211, p. 115 252, Jan. 2020, ISSN: 00092509.

[73] H. Hou, Z. Yuan, Z. Hu, S. Gao, and X. Wu, "Effects of the surface tension gradient and viscosity on coalescence-induced droplet jumping on superamphiphobic surfaces," *Physics of Fluids*, vol. 33, no. 11, p. 112 101, Nov. 2021, ISSN: 10897666.

[74] B. Lafaurie, C. Nardone, R. Scardovelli, S. Zaleski, and G. Zanetti, "Modelling Merging and Fragmentation in Multiphase Flows with SURFER," *Journal of Computational Physics*, vol. 113, no. 1, pp. 134–147, Jul. 1994, ISSN: 0021-9991.

[75] S. Farokhirad, J. F. Morris, and T. Lee, "Coalescence-induced jumping of droplet: Inertia and viscosity effects," *Physics of Fluids*, vol. 27, no. 10, p. 102 102, Oct. 2015, ISSN: 1070-6631.

[76] X. Liu and P. Cheng, "3D multiphase lattice Boltzmann simulations for morphological effects on self-propelled jumping of droplets on textured superhydrophobic surfaces," *International Communications in Heat and Mass Transfer*, vol. 64, pp. 7–13, 2015, ISSN: 07351933.

[77] Z. Khatir, K. J. Kubiak, P. K. Jimack, and T. G. Mathia, "Dropwise condensation heat transfer process optimisation on superhydrophobic surfaces using a multi-disciplinary approach," *Applied Thermal Engineering*, vol. 106, pp. 1337–1344, 2016, ISSN: 13594311.

[78] K. Wang, Q. Liang, R. Jiang, Y. Zheng, Z. Lan, and X. Ma, "Numerical Simulation of Coalescence-Induced Jumping of Multidroplets on Superhydrophobic Surfaces: Initial Droplet Arrangement Effect," *Langmuir*, vol. 33, no. 25, pp. 6258–6268, Jun. 2017, ISSN: 15205827.

[79] X. Chen, J. Lu, and G. Tryggvason, "Numerical simulation of self-propelled non-equal sized droplets," *Physics of Fluids*, vol. 31, no. 5, p. 052 107, May 2019, ISSN: 1070-6631.

[80] M. K. Kim, H. Cha, P. Birbarah, *et al.*, "Enhanced Jumping-Droplet Departure," *Langmuir*, vol. 31, no. 49, pp. 13 452–13 466, Nov. 2015, ISSN: 15205827.

[81] T. Mouterde, T.-V. Nguyen, H. Takahashi, C. Clanet, I. Shimoyama, and D. Quéré, "How merging droplets jump off a superhydrophobic surface: Measurements and model," *Physical Review Fluids*, vol. 2, no. 11, p. 112 001, Nov. 2017, ISSN: 2469-990X.

[82] K. Wang, Q. Liang, R. Jiang, Y. Zheng, Z. Lan, and X. Ma, "Morphology evolution and dynamics of droplet coalescence on superhydrophobic surfaces," *AIChE Journal*, vol. 64, no. 7, pp. 2913–2921, Jul. 2018, ISSN: 0001-1541.

[83] R. Enright, N. Miljkovic, J. Sprittles, K. Nolan, R. Mitchell, and E. N. Wang, "How coalescing droplets jump," *ACS Nano*, vol. 8, no. 10, pp. 10 352–10 362, 2014, ISSN: 1936086X.

[84] M. Bussmann, J. Mostaghimi, and S. Chandra, "On a three-dimensional volume tracking model of droplet impact," *Physics of Fluids*, vol. 11, no. 6, pp. 1406–1417, May 1999, ISSN: 10706631.

[85] S. Farokhirad and T. Lee, "Computational study of microparticle effect on self-propelled jumping of droplets from superhydrophobic substrates," *International Journal of Multiphase Flow*, vol. 95, pp. 220–234, 2017, ISSN: 03019322.

[86] K. W. Connington, T. Lee, and J. F. Morris, "Interaction of fluid interfaces with immersed solid particles using the lattice Boltzmann method for liquid–gas–particle systems," *Journal of Computational Physics*, vol. 283, pp. 453–477, Feb. 2015, ISSN: 00219991.

[87] J. U. Brackbill, D. B. Kothe, and C. Zemach, "A continuum method for modeling surface tension," *Journal of Computational Physics*, vol. 100, no. 2, pp. 335–354, 1992, ISSN: 10902716.

[88] C. M. Rhie and W. L. Chow, "Numerical study of the turbulent flow past an airfoil with trailing edge separation," *AIAA Journal*, vol. 21, no. 11, pp. 1525–1532, May 1983, ISSN: 00011452.

[89] M. M. Francois, S. J. Cummins, E. D. Dendy, D. B. Kothe, J. M. Sicilian, and M. W. Williams, "A balanced-force algorithm for continuous and sharp interfacial surface tension models within a volume tracking framework," *Journal of Computational Physics*, vol. 213, no. 1, pp. 141–173, Mar. 2006, ISSN: 00219991.

[90] S. V. Patankar, *Numerical Heat Transfer and Fluid Flow*. CRC Press, Taylor & Francis Group, Oct. 1980.

[91] J. Göhl, A. Mark, S. Sasic, and F. Edelvik, "An immersed boundary based dynamic contact angle framework for handling complex surfaces of mixed wettabilities," *International Journal of Multiphase Flow*, vol. 109, pp. 164–177, 2018, ISSN: 03019322.

[92] S. F. Kistler, "Hydrodynamics of wetting," *Wettability*, vol. 6, pp. 311–430, 1993.

[93] R. L. Hoffman, "A study of the advancing interface. II. Theoretical prediction of the dynamic contact angle in liquid-gas systems," *Journal of Colloid And Interface Science*, vol. 94, no. 2, pp. 470–486, Aug. 1983, ISSN: 00219797.

[94] M. Jiang and B. Zhou, "Improvement and further investigation on Hoffman-function-based dynamic contact angle model," *International Journal of Hydrogen Energy*, vol. 44, no. 31, pp. 16 898–16 908, 2019, ISSN: 03603199.

[95] P. A. Kralchevsky and K. Nagayama, "Capillary interactions between particles bound to interfaces, liquid films and biomembranes," *Advances in Colloid and Interface Science*, vol. 85, no. 2-3, pp. 145–192, Mar. 2000, ISSN: 0001-8686.

[96] A. Marchand, J. H. Weijs, J. H. Snoeijer, and B. Andreotti, "Why is surface tension a force parallel to the interface?" *American Journal of Physics*, vol. 79, no. 10, pp. 999–1008, Oct. 2011, ISSN: 0002-9505.

[97] K. Washino, H. Tan, M. Hounslow, and A. Salman, "A new capillary force model implemented in micro-scale CFD–DEM coupling for wet granulation," *Chemical Engineering Science*, vol. 93, pp. 197–205, Apr. 2013, ISSN: 00092509.

[98] G. T. Nguyen, E. L. Chan, T. Tsuji, T. Tanaka, and K. Washino, "Interface control for resolved CFD-DEM with capillary interactions," *Advanced Powder Technology*, vol. 32, no. 5, pp. 1410–1425, May 2021, ISSN: 09218831.

[99] N. M. Newmark and F. Asce, "A Method of Computation for Structural Dynamics," *Journal of the Engineering Mechanics Division*, vol. 85, no. 3, pp. 67–94, Jul. 1959, ISSN: 0044-7951.